Loss of Bcl6 transcriptionally alters classical dendritic cells and diminishes T follicular helper cell and Th17-inducing cDC2 in mice

Hongkui Xiao[1,*], Isabel Ulmert[1,*], Luisa Bach[2], Johanna Huber[3], Hamsa Narasimhan[4,5], Ilia Kurochkin[6,7], Yinshui Chang[2,3], Signe Holst[1], Urs Mörbe[1], Lili Zhang[8], Andreas Schlitzer[8], Filipe Pereira[6,7,9], Barbara U. Schraml[4,5], Dirk Baumjohann[2,3], Katharina Lahl[1,10, 11, 12]

Affiliations:

[1]Section for Experimental and Translational Immunology, Institute for Health Technology, Technical University of Denmark (DTU), 2800 Kongens Lyngby, Denmark

[2]Medical Clinic III for Oncology, Hematology, Immuno-Oncology and Rheumatology, University Hospital Bonn, University of Bonn, Bonn, Germany.

[3]Institute for Immunology, Biomedical Center, Faculty of Medicine, LMU Munich, Planegg-Martinsried, Germany.

[4]Biomedical Center, Institute of Cardiovascular Physiology and Pathophysiology, Faculty of Medicine, Ludwig-Maximillians-Universität München, Planegg-Martinsried, Germany.

[5]Walter-Brendel-Centre of Experimental Medicine, University Hospital, LMU Munich, Planegg-Martinsried, Germany

[6]Cell Reprogramming in Hematopoiesis and Immunity Laboratory, Lund Stem Cell Center, Molecular Medicine and Gene Therapy, Lund University, Lund, Sweden.

[7]Wallenberg Center for Molecular Medicine, Lund University, Lund, Sweden.

[8]Quantitative Systems Biology, Life and Medical Sciences (LIMES) Institute, University of Bonn, Germany.

[9]Center for Neuroscience and Cell Biology, University of Coimbra, Coimbra, Portugal.

[10]Immunology Section, Lund University, Lund 221 84, Sweden

[11]Calvin, Phoebe and Joan Snyder Institute for Chronic Diseases, University of Calgary, Calgary, Alberta, Canada.

[12]Department of Microbiology, Immunology, and Infectious Diseases, Cumming School of Medicine, University of Calgary, Calgary, Alberta, Canada.

*these authors contributed equally to this work

Corresponding authors: Katharina Lahl (katharina.lahl@ucalgary.ca) and Dirk Baumjohann (dirk.baumjohann@uni-bonn.de)

Keywords: dendritic cells, transcriptional regulation, Bcl6, cDC1, cDC2, Tfh, Tfr

ABSTRACT

Conventional dendritic cells (cDC) play key roles in immune induction, but what drives their heterogeneity and functional specialization is still ill-defined. Here we show that deletion of the transcriptional repressor Bcl6 in murine cDC alters the phenotype and transcriptome of cDC1 and cDC2, while their lineage identity is preserved. Bcl6-deficient cDC1 were diminished in the periphery but maintained their ability to cross-present antigen to $CD8^+$ T cells, confirming general maintenance of this subset. Surprisingly, the absence of Bcl6 in cDC caused a complete loss of Notch2-dependent cDC2 in the spleen and intestinal lamina propria. DC-targeted Bcl6-deficient mice induced fewer T follicular helper and T follicular regulatory cells in response to immunization and mounted diminished Th17 immunity to *Citrobacter rodentium* in the colon. Our findings establish Bcl6 as an essential transcription factor for subsets of cDC and add to our understanding of the transcriptional landscape underlying cDC heterogeneity.

INTRODUCTION

Conventional dendritic cells (cDC) have the unique ability to present antigen to naïve T cells within lymphoid organs[1–3]. Upon encounter of antigen, migratory cDC scanning the peripheral environment mature and relocate to the draining lymph nodes (LNs), where they collaborate with LN-resident cDC to initiate immunity[4]. The spleen is the secondary lymphoid organ responsible for induction of immune responses to blood-derived antigen[5] and maturation of splenic cDC leads to similar relocation from the marginal zone and red pulp into the white pulp, where naïve B and T cells reside[6,7]. “Resident” resting DC are also found in the spleen, where they are located in the T cell zones in the absence of stimulation[8].

Conventional DC are broadly divided into two main subsets, cDC1 and cDC2[1]. cDC1 are characterized by their expression of the cDC1-exclusive chemokine receptor XCR1 and the absence of CD11b and Sirpα. Their development and functions are dependent on the transcription factors (TFs) IRF8[9,10], BATF3[11], Nfil3[12,13] and Id2[14] and they excel at cross-presenting antigen to CD8$^+$ T cells, which is at least in part attributable to their ability to engulf apoptotic material[15–19]. cDC2 express high levels of CD11b and Sirpα, but not XCR1, and the transcriptional network governing their development is less well defined. cDC2 show a higher level of heterogeneity than cDC1[20] and recent attempts to subset cDC2 further have suggested separation based on Notch2 versus Klf4-dependency[21]. IRF4-deficiency leads to a partial loss of cDC2 and is thought to impact primarily on their survival and ability to migrate[22–24]. Other TFs reported to influence cDC2 development or function include ZEB2[25], IRF-2[26] and Rel-B[27]. In the spleen, the majority of cDC2 express endothelial cell specific adhesion marker (ESAM), a marker defining cDC2 located in the bridging channels of the marginal zone, where they fulfill critical functions in activating CD4$^+$ T cells and germinal center (GC) formation[28,29]. The development of ESAM^{hi} cDC2 depends on Notch2-signaling induced by delta ligand 1 (DLL1) expressed by stromal cells[22,28,30,31] and on the chemokine receptor Ebi2 (GPR183)[32].

The TF Bcl6 plays an essential role in GC reactions, being required for the differentiation of both GC B cells and T follicular helper (Tfh) cells in a cell intrinsic manner[33]. Bcl6 is expressed in cDC1, and to a lower extent in cDC2[20] and we have shown previously that complete Bcl6-deficiency causes a loss of CD11b$^-$ DC, presumed to be cDC1[20]. Other work has confirmed that Bcl6-deficient mice lack splenic CD8-expressing cDC1, but also reported a reduction in splenic CD4$^+$ cDC2[34]. However, a more recent study has disputed these findings, by showing normal cDC1 numbers in mice with conditional *Bcl6* deletion driven by cre recombinase under the control of the *Csf1* promoter. Importantly, these authors suggested that down-regulation of CD11c in the absence of Bcl6 may have compromised the detection of cDC1 in the earlier studies[35].

Here we reconcile these conflicting data by performing in-depth analysis of the cDC compartment in mice lacking Bcl6 in all cDC or specifically in cDC1, using CD11c- and Clec9a- or XCR1-driven cre drivers, respectively. Our results show that while cDC1 showed substantial alterations in gene expression including deregulation of genes involved in cytokine signaling and cell adhesion, their

ability to cross-present antigen was largely conserved in the absence of Bcl6. Bcl6-deficiency in DC led to a complete loss of the Notch2-dependent ESAM^{hi} cDC2 subset in the spleen and consequently to alterations in splenic Tfh and T follicular regulatory (Tfr) cells as well as antibody responses following immunization. Likewise, Notch2-dependent cDC2 in the intestinal lamina propria (LP) were reduced in the absence of Bcl6 in DC, leading to a decrease in Th17-responses and delayed healing upon infection with the enteric pathogen *Citrobacter rodentium*. Our findings suggest that the core subset identities of cDC1 and cDC2 are maintained in the absence of Bcl6, but that its deficiency in DC causes cell-intrinsic, subset-specific alterations in DC abundance and function, which translates into corresponding defects in adaptive immune responses.

RESULTS

Bcl6 deficiency alters DC subset phenotypes and numbers across tissues

We have previously shown that mice completely lacking Bcl6 are largely devoid of CD11b^{-} cDC, presumed to be cDC1[20]. To better define the impact of Bcl6-deficiency on cDC1, we generated mice lacking Bcl6 specifically in cDC1 by crossing XCR1.cre mice to mice carrying a floxed Bcl6 gene (*XCR1.Bcl6^{KO}*). Additionally, we deleted Bcl6 in all CD11c-expressing cells by crossing CD11c.cre mice to Bcl6^{flox} mice (*CD11c.Bcl6^{KO}*). As controls, we used the respective cre negative Bcl6^{flox} littermates (designated as control throughout). As expected, flow cytometry revealed mutually exclusive populations of CD11c^{+}MHCII^{+} cDC in control spleens based on the expression of XCR1 or CD11b to identify cDC1 and cDC2, respectively. However, there was a clear population of XCR1^{+}CD11b^{+} cDC in the absence of Bcl6 in the spleens of both Bcl6-deficient mouse lines (Fig. 1A, for complete gating strategies see Suppl. Fig. 1). XCR1^{+}CD11b^{+} cDC were also abundant within the resident populations of peripheral and mesenteric lymph node (pLN and mLN) cDC in the absence of Bcl6 (Fig. 1B). The absolute numbers of total XCR1^{+} cDC (independent of CD11b expression) were only mildly reduced in *XCR1.Bcl6^{KO}* and normal in *CD11c.Bcl6^{KO}* mice, while XCR1^{-}CD11b^{+} cDC were significantly diminished in *CD11c.Bcl6^{KO}* mice, but normal in *XCR1.Bcl6^{KO}*

mice (Fig. 1A). Resident cDC numbers were not substantially altered in either pLNs or mLNs (Fig. 1B).

We next analyzed migratory DC populations in different organs. Mice lacking Bcl6 in cDC1 or in all DC had significantly fewer migratory XCR1$^+$ cDC in pLNs and mLNs and these also expressed CD11b (Fig. 2A, for complete gating strategies see Suppl. Fig. 1). Interestingly, we also detected a loss of XCR1$^-$CD11b$^+$CD103$^+$ cDC in the migratory compartment of the mLNs of *CD11c.Bcl6*^{KO} mice, whereas the numbers of XCR1$^-$CD11b$^+$CD103$^-$ cDC were normal (Fig. 2A). As the majority of migratory cDC in the mLNs derives from the small intestinal lamina propria (SILP), we next analyzed this compartment. There were fewer XCR1$^+$ cDC in the SILP of both *XCR1.Bcl6*^{KO} and *CD11c.Bcl6*^{KO} mice, all of which again expressed CD11b (Fig. 2B). In addition, the numbers of XCR1$^-$CD11b$^+$CD103$^+$ cDC were reduced in *CD11c.Bcl6*^{KO} mice, while the numbers of XCR1$^-$CD11b$^+$CD103$^-$ cDC were less affected (Fig. 2B). Together these results suggest that the decreases in migratory XCR1$^+$ and XCR1$^-$CD11b$^+$CD103$^+$ cDC seen in mLNs are caused by absence of these populations, rather than a disability to migrate. Similar changes in cDC were seen in the lung and the blood in the absence of Bcl6, with reduced numbers and upregulation of CD11b in XCR1$^+$ cDC in both *XCR1.Bcl6*^{KO} and *CD11c.Bcl6*^{KO} mice, together with reduced numbers of XCR1$^-$CD11b$^+$ cDC in *CD11c.Bcl6*^{KO} mice (Suppl. Fig. 2). Interestingly, while XCR1$^+$ DCs upregulated CD11b in all organs, XCR1$^-$CD11b$^+$ DCs further upregulated CD11b particularly in systemic populations (spleen and resident DCs from the mLN and pLN), while peripheral XCR1$^-$CD11b$^+$ DC showed no further increase of their naturally high levels of CD11b (Suppl. Fig. 3). Thus, Bcl6 deficiency affects cDC in several locations.

cDC1 and cDC2 signatures are preserved in the absence of Bcl6 in DC

One of the most surprising findings from our studies was the expression of the cDC2 marker CD11b by the XCR1$^+$ cDC that was preserved in Bcl6-deficient mice. To determine whether this reflects acquisition of CD11b by cDC1, or cDC2 with aberrant XCR1 expression, we sorted splenic XCR1$^+$ cDC (independent of CD11b expression) and XCR1$^-$CD11b$^+$ cDC from control, *XCR1.Bcl6*^{KO} and *CD11c.Bcl6*^{KO} mice for bulk mRNA-sequencing (see Fig. 1A for gating). Principal component

(PC) analysis showed that XCR1$^+$ cDC segregated from XCR1$^-$CD11b$^+$ cDC in all mouse models along PC axis 1, which accounted for 69% of the variance. This strongly supports the idea that Bcl6-deficient cDC1 and cDC2 maintained overall lineage identity (Fig. 3A). Nevertheless, PC2 separated the populations on the basis of Bcl6 presence or absence, accounting for 13% of the variance and suggesting that Bcl6 has a significant impact on the gene transcription profile of both cDC1 and cDC2. Interestingly, cDC1 from *XCR1.Bcl6^{KO}* and *CD11c.Bcl6^{KO}* mice clustered closely and were separated from control cDC1, while cDC2 in *CD11c.Bcl6^{KO}* mice segregated from those in *XCR1.Bcl6^{KO}* and control mice, consistent with XCR1-cre being specific to cDC1 and indicating that Bcl6 regulates gene expression in both cDC subsets in a cell-intrinsic manner. PC3 accounted for 4% of the variance and showed opposite directional bias in Bcl6-deficient cDC1 and cDC2 (Fig. 3A). This suggests that Bcl6-mediated regulation of gene transcription may affect some targets in cDC1 and cDC2 differently.

To explore further how Bcl6 might regulate cDC lineage identity, we generated cDC1 and cDC2 signatures by identifying the top 50 genes that were differentially expressed between our control cDC1 and cDC2 and interrogated how these signatures were affected by a loss of Bcl6 expression (for gene lists and expression levels see Suppl. Table 1). Supporting their maintenance of lineage identity, XCR1$^+$ cDC from both *XCR1.Bcl6^{KO}* and *CD11c.Bcl6^{KO}* mice retained the expression of cDC1 markers, including *Irf8*, *Tlr3*, *Clec9a*, and *Cadm1* (Fig. 3B). However, *Cd8a* was downregulated in Bcl6-deficient XCR1$^+$ cDC and several genes associated with cDC2 identity were upregulated by XCR1$^+$ cDC in the absence of Bcl6, including *Sirpa*, *Zeb2*, *Csf1r* and *Itgam* (encoding CD11b) (foldchange > 2, padjust < 0.01). Although Bcl6-deficient CD11b$^+$ cDC2 did not express cDC1 specific markers, cDC2 from *CD11c.Bcl6^{KO}* mice showed altered expression of several classical cDC2 markers, of which some were further upregulated such as *Csf1*, *Zeb2* and *Itgam*, while others were downregulated, including *Clec4a4* and *CD4* (Fig. 3B). Despite maintenance of core lineage expression patterns, the overall transcriptional profiles of XCR1$^+$ and XCR1$^-$CD11b$^+$ cDC were significantly altered in the absence of Bcl6 (Fig. 3A, C). In total, 607 genes were differentially regulated in XCR1$^+$ cDC from *XCR1.Bcl6^{KO}* mice compared with control cDC1, with 473 being upregulated and 134 downregulated. In contrast, of the 452 differentially regulated genes in cDC2 from *CD11c.Bcl6^{KO}* mice, only 206 were upregulated, compared with 246

downregulated genes (Fig. 3D, for list of contributing genes see Suppl. Table 2). Interestingly, only 79 genes were coordinately overexpressed in Bcl6-deficient cDC1 and cDC2, and 32 genes were coordinately downregulated in the absence of Bcl6 in both subsets. 12 genes were reciprocally regulated in the two subsets, of which 11 genes were upregulated in cDC1 and downregulated in cDC2 (including receptor encoding genes *Ffar1* and *Lair1,* enzyme-encoding genes *Tgm2, Pigv* and *Malt1* and genes encoding proteins implicated in cellular and intracellular adhesion and transport *Cdh17, Ctnnd2, Ston2 and Rin2*). The gene for the actin-binding protein Plectin was the only gene upregulated in cDC2 and downregulated in cDC1. Taken together, although the lineage identity of splenic cDC1 and cDC2 is generally maintained in the absence of Bcl6, this does result in significant changes in subset-specific gene expression in both cDC subsets.

Bcl6-deficient cDC1 maintain the ability to cross-present antigen

To better characterize the impact of Bcl6-deficiency on cDC1, we next compared the expression of cDC1-related markers using flow cytometry. This confirmed the maintenance of Tlr3, Xcr1, Irf8, CD103 and Clec9a expression by XCR1$^+$ cDC from the spleen of *XCR1.Bcl6^{KO}* mice, as well as upregulation of CD11b and Sirpα and loss of CD8α (Fig. 4A). In addition, we detected higher expression of the costimulatory ligand CD24 on Bcl6-deficient cDC1.

The most characteristic property of cDC1 is to cross-present exogenous antigen to class I MHC-restricted CD8$^+$ T cells, a function which involves cell-surface receptors such as Clec9A (Dngr1) that mediate the uptake of dead cells[18,19]. Our gene expression analysis suggested that XCR1$^+$ cDC1 maintained the expression of *Clec9a* in the absence of Bcl6 and this was confirmed by flow cytometry (Fig. 4A). We therefore examined whether cross-presentation was intact in *XCR1.Bcl6^{KO}* animals by injecting heat-killed ovalbumin-expressing mouse embryonic fibroblasts (OVA-MEFs) into recipient mice adoptively transferred with OVA-specific TCR-transgenic CD8$^+$ T cells from OT-I mice. OT-I cell proliferation strictly depends on cDC1-mediated cross-presentation in this model[17]. OT-I cells proliferated to a similar extent in the spleens of OVA-MEF-injected *XCR1.Bcl6^{KO}* and control mice (Fig. 4B, C), suggesting that Bcl6-deficient cDC1 retain their ability to cross-present. OT-I cell proliferation was also observed in the mLN. In the mLN of *XCR1.Bcl6^{KO}*

mice OT-I cells showed somewhat diminished proliferation compared to control mice. This most likely reflects the decreased number of migratory cDC1 in the mLN of *XCR1.Bcl6*^{KO} mice (Fig. 2A), as mLN cDC1 from *XCR1.Bcl6*^{KO} cross-presented antigen with comparable efficiency as control cDC1 in an *in vitro* cross-presentation assay upon cDC1-input normalization (Suppl. Fig. 4).

Bcl6-deficiency in cDC1 causes alterations in immunologically relevant pathways

For a broader assessment of whether the absence of Bcl6 influences the immunological functions of cDC1, we next performed gene set enrichment analysis of the RNA-Seq data from XCR1^{+} cDC in *XCR1.Bcl6*^{KO} and control mice. This showed that several immunologically relevant gene ontology pathways were enriched within the differentially expressed gene sets, including *leukocyte adhesion*, *proliferation* and *activation*, as well as *production of IL-1* (Fig. 5A). In parallel, KEGG pathway analysis highlighted differences in *cytokine-cytokine receptor interactions, NOD-like receptor signaling pathway, MERK signaling pathway, hematopoiesis cell lineage, Tuberculosis* and *C-type lectin receptor signaling pathway* (Fig. 5B, C). Upregulated genes were generally enriched for pro-inflammatory signals, and among others, we found an over-representation of genes involved in the IL-6 pathway in cDC1 from *XCR1.Bcl6*^{KO} mice (Suppl. Fig. 5). Interestingly, we detected higher levels of serum IL-6 in *XCR1.Bcl6*^{KO} mice injected with the double-stranded RNA-mimic poly(I:C) when compared to treated controls (Fig. 5D). These data suggest that Bcl6-mediated transcriptional repression in cDC1 may tune the function of this subset.

Taken together, although cDC1-specific Bcl6 deficiency alters the phenotype and transcriptional profile of cDC1, the hallmark function of cDC1 to cross-present antigen is largely unaffected by the loss of Bcl6.

Bcl6-deficiency results in a selective loss of Notch2-dependent cDC2

In addition to its role in cDC1, our initial results also revealed a significant role for Bcl6 in the gene expression signature of cDC2. Furthermore, the numbers of cDC2 were reduced in the spleen of

CD11c.Bcl6^{KO} mice, as were the numbers of cDC2 expressing CD103 in the intestinal LP and mLNs. Diminished cDC2 numbers in the blood of CD11c.Bcl6^{KO} mice suggest that this was not due to a release of cDC2 into the bloodstream (Suppl. Fig. 2B). The remaining cDC in the spleen of *CD11c.Bcl6^{KO}* mice also showed somewhat lower expression of MHCII and higher expression of CD11b than control cDC2 (Fig. 6A). Further phenotyping of spleen cDC2 in *CD11c.Bcl6^{KO}* mice revealed a striking loss of the ESAM^{hi} cDC2 subset (Fig 6B and Suppl. Fig. 2). We verified our findings in an independent mouse model in which Bcl6 deletion was induced by cre recombinase under the control of the *Clec9a* promoter, which targets cDC precursors and their progeny and some pDCs but no other leukocytes[36]. These mice additionally carry a YFP reporter following a floxed stop cassette in the ubiquitous ROSA26 locus to monitor targeting efficiency. As in *CD11c.Bcl6^{KO}* mice, spleen cDC in *Clec9a.Bcl6^{KO}* mice showed altered CD11b expression and loss of ESAM^{hi} cDC2 (Fig. 6C, D and Suppl. Fig. 6). This was apparent in the analysis of bulk cDC2 in *Clec9a.Bcl6^{KO}* mice and was even more pronounced when pre-gating on YFP^{+} instead of CD11c, which enriches cDC2 with a history of *Clec9a*-promoter activity (Fig. 6E). Importantly, this also shows that CD11c down-regulation in the absence of Bcl6 does not account for the reported phenotype (for side-by-side comparison of CD11c- and Clec9A-reporter-based gating strategies see Suppl. Fig. 7).

As expected[28], the ESAM^{lo} subset of cDC2 expressed slightly lower levels of CD11c compared to their ESAM^{hi} counterparts and a significant proportion lacked expression of 33D1 and CD4, which were expressed uniformly by ESAM^{hi} cDC2 (Fig. 6F). The total population of cDC2 remaining in *CD11c.Bcl6^{KO}* mice resembled the ESAM^{lo} population in terms of these markers but expressed higher levels of CD11b and IRF4 than either ESAM^{hi} or ESAM^{lo} control cDC2 subset, suggesting these markers may be specific targets of Bcl6 repression.

To explore the nature of the cDC2 remaining in the spleen of *CD11c.Bcl6^{KO}* mice further, we performed gene set enrichment analysis (GSEA) of differentially expressed genes between *CD11c.Bcl6^{KO}* and control cDC2 in gene sets derived from publicly available bulk RNA-Seq data from ESAM^{hi} and ESAM^{lo} cDC2 from control spleen[37]. As expected from their usual predominance in control spleen, control cDC2 gene signatures were highly enriched in ESAM^{hi} vs ESAM^{lo} gene sets, while *CD11c.Bcl6^{KO}* cDC2 gene signatures were highly enriched in ESAM^{lo} vs ESAM^{hi} gene

sets (Fig. 7A). We next directly compared the set of genes that was differentially expressed in ESAM^{hi} vs ESAM^{lo} cDC2 with the gene set differentially expressed in *CD11c.Bcl6^{KO}* vs control cDC2. In accordance with the GSEA data, the majority of the top 50 genes expressed more prominently by ESAM^{hi} cDC2 were also significantly over-represented in the population of total control cDC2, which expressed much fewer of the top 50 genes from ESAM^{lo} cDC2 (Fig. 7B). Conversely, the genes over-expressed by total cDC2 from *CD11c.Bcl6^{KO}* spleen showed much more overlap with the top 50 genes expressed by ESAM^{lo} cDC2, while the genes over-expressed by ESAM^{hi} cDC2 were mostly downregulated in Bcl6-deficient cDC2 (Fig. 7B, for a complete gene list containing expression levels see Suppl. Table 3). These data confirm that Bcl6 deficiency in DC causes the loss of the ESAM^{hi} lineage of splenic cDC2.

DC-specific loss of Bcl6 causes defects in T follicular helper cell priming in the spleen

ESAM^{hi} spleen DC reside in the marginal zone bridging channels, where they play a prominent role in the induction of germinal centers[29]. Confocal microscopy using CD11c as a pan-DC marker and TLR3 and Sirpα to define cDC1 and cDC2, respectively, confirmed a substantial loss of DC from this region in the *CD11c.Bcl6^{KO}* spleen (Fig. 8A). This was also evident in *Clec9a.Bcl6^{KO}* and *Clec9a.Bcl6^{WT}* control mice carrying a YFP reporter under the control of the *Clec9a* promoter, in which Bcl6-deficiency in DCs led to a similar decrease in marginal zone bridging channel DCs (Fig. 8B). To test the functional relevance of this defect, we adoptively transferred OVA-specific TCR-transgenic CD4^{+} T cells (OT-II) into control and *CD11c.Bcl6^{KO}* mice, immunized the mice with OVA + poly(I:C) intraperitoneally and assessed the generation of antigen-specific Tfh cells three days later (Suppl. Fig. 8A). We chose this timepoint because this early Tfh cell induction is independent of GC B cells[38,39], which are known to express CD11c and are required for the maintenance of Tfh cells at later times[40]. Although OT-II cells expanded normally in the *CD11c.Bcl6^{KO}* mice in response to immunization, the early induction of antigen-specific CXCR5^{+}Bcl6^{+} Tfh cells was markedly reduced in immunized *CD11c.Bcl6^{KO}* mice compared to control mice (Suppl. Fig. 8A), suggesting that Bcl6-dependent cDC indeed drive early Tfh cell induction in this model. To enable analysis of later timepoints of the Tfh cell response and to confirm our findings in mice in which Bcl6 deletion

is confined to cDC, we next adoptively transferred naïve OT-II cells into *Clec9a.Bcl6*^{WT} control or *Clec9a.Bcl6*^{KO} mice, followed by i.p. immunization with NP-OVA in alum adjuvants and analysis of the spleen seven days later (Fig. 8C). The frequency of CXCR5^{+}PD-1^{+} and CXCR5^{+}Bcl6^{+} Tfh cells was significantly reduced in OT-II cells recovered from *Clec9a.Bcl6*^{KO} hosts as compared to control animals (Fig. 8D and Suppl. Fig. 8B). To better assess the long-term effects of DC-restricted Bcl6 deficiency on Tfh cell and humoral immune responses, we immunized *Clec9a.Bcl6*^{WT} and *Clec9a.Bcl6*^{KO} mice i.p. with NP-KLH/alum and analyzed the spleens two weeks later (Fig. 8E). Total spleen cellularity was not significantly increased in *Clec9a.Bcl6*^{KO} mice (Fig. 8F). As regulatory T (Treg) cells do not develop from naive OT-II precursor cells, such as in the previous adoptive transfer experimental setting, and Tfr cells share similarities with Treg cells and Tfh cells[41,42], such as expression of Foxp3 and Bcl6, respectively, we quantified all three subsets within the endogenous T cell compartment following NP-KLH/alum immunization. Total numbers of Foxp3^{-} and Foxp3^{+} CD4^{+} T cells were not affected by DC-restricted Bcl6 deficiency (Fig. 8F and Suppl. Fig. 8C). While the frequencies of endogenous CXCR5^{int}PD-1^{int} and CXCR5^{int}Bcl6^{int} Tfh cells were reduced among conventional Foxp3^{-} CD4^{+} T cells of the conditional knockout mice, the frequencies of GC Tfh cells, gated as CXCR5^{hi}PD-1^{hi} or CXCR5^{hi}Bcl6^{hi}, were not altered in *Clec9a.Bcl6*^{KO} mice at day 14 after immunization (Fig. 8G, H). In contrast, we observed a strong reduction in CXCR5^{hi}PD-1^{hi} or CXCR5^{hi}Bcl6^{hi} Tfr cells among Foxp3^{+} CD4^{+} T cells (Fig. 8G, H), indicating that Bcl6 in DCs is particularly important for the generation of Tfr cells. To address the impact of DC-restricted Bcl6 deficiency on the antibody response, we assessed the NP-specific serum antibody levels at different time points following NP-KLH/alum immunization (Fig. 8 I), focusing on total IgG and the signature isotype induced by type-2 immunization with alum adjuvants, IgG1. Quantifying both the amounts of NP-specific antibodies against NP_{36}-coated BSA, a proxy for total NP-binding antibodies, as well as against NP_{2}-coated BSA, a proxy for high-affinity NP-binding antibodies, we found reduced NP-specific antibody responses in *Clec9a.Bcl6*^{KO} mice (Fig. 8 J and Suppl. Fig. 8D). In conclusion, Bcl6 deficiency in cDC causes the loss of ESAM^{hi} cDC2 and impairs Tfh, Tfr, and antibody responses in the spleen.

DC-specific loss of Bcl6 causes defects in Th17 cell priming in the colon of mice infected with *C. rodentium*

In addition to their role in driving GC reactions in the spleen, Notch2-dependent cDC2 have been shown to support Th17-dependent immunity towards *C. rodentium* in the colon[22]. The colonic LP (cLP) of *CD11c.Bcl6*^{KO} mice contained significantly fewer cDC than that of control mice, with the most pronounced loss detected in the CD103^{+} cDC2 population (Fig. 9A, B). To analyze whether Bcl6-deficiency recapitulated the functional consequences of Notch2-deficiency, we infected *CD11c.Bcl6*^{KO} and control littermates with *C. rodentium. CD11c.Bcl6*^{KO} mice lost comparable weight to control littermates early after infection, with delayed recovery as evidenced by significantly lower body weight from day 11 onwards (Fig. 9C). Consistent with a lack in weight difference between genotypes at day nine post infection, colon length and bacterial load were comparable at this time point, while there was a tendency towards shorter colons and elevated bacterial load in *CD11c.Bcl6*^{KO} mice compared to control littermates 21 days post infection (Fig. 9C). At this late stage during infection, colons from *CD11c.Bcl6*^{KO} mice continued to show mild pathology, while control littermates appeared fully healed (Fig. 9D). In parallel, there were blunted Th17 responses in the cLP of *CD11c.Bcl6*^{KO} mice 9 days after *C. rodentium* infection (Fig. 9E, gating strategies depicted in Suppl. Fig. 9), while Th1 and Treg numbers were not affected. This defect in Th17 priming was no longer evident 21 days after infection (Fig. 9F). To address whether our results were due to a lack of Bcl6 in *bona fide* DCs, we infected *Clec9a.Bcl6*^{KO} mice and controls with *C. rodentium* and analyzed their CD4 T cell compartment on day 9 post infection. While we detected a trend towards lower RORγt^{+} CD4 T cell numbers, Tbet^{+} and Foxp3^{+} CD4 T cells were more prominently affected (Suppl. Fig. 10A). Analysis of YFP expression as a surrogate of *Clec9a.cre* activity in intestinal DCs in *Clec9a.Bcl6*^{KO} mice however revealed only partial targeting of cDC2 in the gut, potentially explaining the moderate deficiency in Th17 priming (Suppl. Fig. 10B).

These data show that Bcl6-deficiency in CD11c$^+$ mononuclear phagocytes causes the loss of a prominent colonic cDC2 subset, with a consequent defect in Th17 priming in response to *C. rodentium* infection, leading to delayed healing and recovery.

DISCUSSION

We show here that Bcl6-deficiency in the DC compartment causes major transcriptional alterations with subset-specific consequences. Specifically, Bcl6-deficient cDC1 acquire a XCR1/CD11b double-positive phenotype not seen in control mice, where XCR1 and CD11b are mutually exclusive markers of cDC1 and cDC2, respectively. However, Bcl6-deficient cDC1 retained a cDC1-like transcriptome, cDC1 lineage markers and the ability to cross-present. The lack of Bcl6 in DC also revealed a critical role for Bcl6 in the development of the ESAM^{hi} subset of cDC2 in the spleen and cDC2 in the intestines and there was a parallel defect in splenic Tfh cell induction in response to protein antigen immunization and in intestinal Th17 induction in response to *C. rodentium* infection. Together these findings extend the role of Bcl6 to the regulation of cDC2 behavior in GC function and the periphery.

We previously described a selective loss of putative cDC1 in the spleen of Bcl6-deficient mice based on the absence of CD8α^+CD11b$^-$ cDC[20]. Here we refine this interpretation by showing that the numbers of resident cDC1 are in fact normal when Bcl6 is lacking in CD11c$^+$ cells or cDC1, but they upregulate CD11b and down-regulate CD8α, causing them to merge into the classical cDC2 gate. In contrast, the numbers of migratory CD11b$^-$ CD103$^+$ cDC1 are decreased in the mLN and intestinal mucosa of mice lacking Bcl6 within the DC compartment, a finding supported by defective cross presentation activity in the mLNs. We currently cannot explain the differential effects of Bcl6 deficiency on resident versus migratory cDC1 populations. However, a similar dichotomy has been described recently for dependence on DC-SCRIPT, whose absence predominantly diminished resident cDC1[43]. As Bcl6 primarily acts as a transcriptional repressor, it is possible that DC-SCRIPT and Bcl6 integrate in a feedback loop to regulate cDC1 migration or survival upon maturation and this idea requires further study.

As Bcl6 is not expressed by DC progenitors in the bone marrow and their frequency is not affected by the lack of Bcl6[35,44], Bcl6 seems to act downstream of other cDC1 lineage specifying TFs such as IRF8, Nfil3, BATF3, DC-SCRIPT, and Id2. In models deficient of those TFs, the cDC1 lineage is affected from the precursor level onwards, preventing their expression of all lineage markers, as well as their ability to cross-present antigen[10,12–14,43,45–48], hallmarks that were preserved in Bcl6-deficient cDC1. Rather, it appears that Bcl6 may fine-tune cDC1 identity by suppressing selected cDC2 genes at the mature state and as a result, Bcl6-deficient cDC1 maintain key cDC1 genes such as XCR1, TLR3, and CLEC9A as well as cross-presentation function. However, they show a gene expression profile that suggests a cDC2-related "gain-of-function", with enhanced expression of genes of the cytokine-cytokine receptor pathway, cell adhesion and migration pathways and pathways associated with inflammasome activity. Interestingly, cDC1 with upregulated CD11b and Sirpα have also been described when the TF ZEB2 is over-expressed from the pre-cDC stage onwards[25]. Exploring how Bcl6 interacts with this and other lineage determining factors to regulate cDC1 gene expression and functions will be an important topic for future research.

CD11c.Bcl6^{KO} and *Clec9a.Bcl6^{KO}* mice lacked the dominant subset of ESAM^{hi} cDC2 in the spleen and comparison of gene expression profiles between ESAM^{hi} and ESAM^{lo} control cDC2 subsets and cDC2 from *CD11c.Bcl6^{KO}* mice showed that Bcl6-deficient cDC2 closely aligned with control ESAM^{lo} cDC2. However, this overlap was not absolute, suggesting that Bcl6-deficiency causes transcriptional changes in all cDC2. For example, the extent of dysregulation of IRF4 and CD11b expression in the absence of Bcl6 cannot solely be explained by the loss of ESAM^{hi} cDC2. In addition, both markers were also upregulated in Bcl6-deficient cDC1, again indicating a wider role for Bcl6 in control of mature cDC differentiation. Interestingly, the consequences of Bcl6 deficiency on cDC overlap with those previously shown for Notch2 deficiency[20,28,34]. Specifically, both mice show deficiencies in cDC1 and ESAM^{hi} cDC2, but it remains to be determined whether the apparent loss of cDC1 in Notch2-deficient animals reflects genuine absence of these cells, or is because their phenotype has simply changed, as we show in Bcl6-deficient mice. Of note, the cDC1 marker CD24 is upregulated in both Bcl6- and Notch2-targeted mice (our study and [22,28]), arguing against a developmental defect within the cDC1 spleen compartment in Notch2-targeting models. It will be of interest to explore how the Notch2- and Bcl6-pathways interact in DC biology.

Consistent with the findings that cDC2 equivalent to the ESAM^{hi} population locate preferentially in marginal zone bridging channels in the spleen[49], the dysregulation in splenic cDC populations in both Bcl6- and Notch2-deficient mice was associated with loss of cDC from this region of the spleen ([29] and current results). Localization of cDC2 to the bridging channels is dependent on the homing receptor GPR183[50,51] and Bcl6 regulates GPR183 expression in B cells[52]. However, GPR183 expression levels were not altered in Bcl6-deficient cDC2, suggesting either that additional factors are required for the correct positioning of cDC2 in the spleen, or that Bcl6-deficiency causes a development block or diminished survival within ESAM^{hi} cDC2 irrespective of their location. Along those lines, GPR183 deficiency in cDC2 specifically diminished antibody response generation to particulate antigen, while responses to soluble antigen were unaffected[51]. The defect in ESAM^{hi} cDC2 we found in *CD11c.Bcl6^{KO}* and *Clec9a.Bcl6^{KO}* mice was accompanied by reduced induction of Tfh cells in response to parenteral immunization with soluble OVA, suggesting a general deficiency in supporting GC reactions in these mice. While it has been suggested that Notch2 is needed to ensure correct positioning of cDC2 for access to antigen in the bloodstream[28], it has to our knowledge not been addressed whether response deficits were limited to particulate antigen in these mice. Further investigation is needed to explore the importance of correct localization on development, survival, and antigen capture by cDC2 and how this might be controlled by a Bcl6-Notch2 axis.

DC-specific deletion of Bcl6 caused alterations in the generation of Tfh cells, Tfr cells, and corresponding antibody responses. As T and B cell-intrinsic expression of Bcl6 is known to be required for Tfh cell and GC B cell differentiation[53,54], our findings extend this concept to the DC stage. Our data indicates that Tfh and Tfr cell fates of activated conventional CD4^{+} T cells and Treg cells, respectively, are predetermined or imprinted by Bcl6 expression patterns already in DCs. One interesting finding was the strong effect of DC-specific Bcl6 deficiency on Tfr cells, which are believed to mainly develop from thymic Tregs[41,42]. Given the stronger reduction in GC Tfh cells in *Clec9a.Bcl6^{KO}* mice at early stages following immunization, as compared to later stages, it is possible that a continued lack of Tfr-mediated suppression of Tfh cells may allow for a compensatory outgrowth of Tfh cells over time, thus mitigating the net effects of DC-specific Bcl6 deficiency. This would be in line with the multistep differentiation process of Tfh cells in which B

cells become the sole antigen-presenting cell subset in GCs, with no classical DCs being present in GCs[55].

XCR1^{-} CD11b^{+}CD103^{+} intestinal LP DC were also reduced in the absence of Bcl6 in DC, again mirroring the phenotype observed in Notch2-deficient mice[22,28]. cDC2 are potent drivers of Th17 responses in the intestines[23,56], but recent findings suggest that DC-independent Th17 cell induction can also occur[57]. As *CD11c.Notch2^{KO}* mice succumb early to *C. rodentium* infection due to deficient IL-23 driven innate immunity, the adaptive immune response has not been investigated in this model[22]. In contrast, the early stages of infection were normal in *CD11c.Bcl6^{KO}* mice, but these mice showed a delay in recovery at later stages and altered kinetics of Th17 induction, with significantly lower Th17 numbers at day nine, which had normalized by day 21. We cannot currently explain the differences in the early innate immune response between *CD11c.Notch2^{KO}* and *CD11c.Bcl6^{KO}* mice, but our data are consistent with the idea that DC play the dominant role in coordinating the adaptive immunity required to terminate infection. However, while Bcl6-dependent cDC2 support optimal Th17 induction to *C. rodentium*, they are not essential for this response, as Th17 numbers normalized over time, possibly due to continuous proliferation in the presence of the pathogen.

Our results show that Bcl6 deficiency does not alter cDC1 and cDC2 lineage identity, but it alters their transcriptional profile and relative abundance of both lineages and their subsets in different tissues. Specifically, although cDC1 in all tissues examined acquired several cDC2 markers in the absence of Bcl6, they retained their transcriptional and functional identity as cDC1. In contrast, Bcl6 deficiency had differing effects on cDC2 subsets that depended on their location and phenotype, with selective depletion of ESAM^{hi} cDC2 in spleen and CD103^{+}CD11b^{+} cDC2 in the intestine. These effects were similar to those described for a deficiency in Notch2 and had significant functional consequences for adaptive immunity in the spleen and intestine. These data add to the emerging and poorly understood heterogeneity within the cDC2 compartment by establishing that certain cDC2 subsets require Bcl6-expression in the DC compartment in addition to Notch2- and lymphotoxin β-signaling. Finally, complementary to its established roles in

controlling B and T cell-intrinsic cell fate decisions[53], our findings establish Bcl6 as a subset-specific regulator of DC development and function with critical consequences for the induction of adaptive immune responses.

MATERIALS AND METHODS

Mice

Xcr1.cre (*B6-Xcr1*^{tm2Ciphe})[58], *CD11c.cre*[31] and *Clec9A.cre*[36] mice were crossed to *Bcl6*$^{fl/fl}$ mice[59] (from Alexander Dent or JAX.org stock number #023727) to obtain DC-specific Bcl6-knockout models. *Clec9A.Bcl6*^{KO} mice and *Clec9A.Bcl6*^{CONTROL} control mice were both maintained homozygous for cre and additionally contained homozygous a *Rosa26*$^{fl\text{-}Stop\text{-}fl\text{-}YFP}$ allele (JAX.org stock number 006148). *CD11c.Bcl6* and *XCR1.Bcl6* models were maintained heterozygous for cre and negative littermates were used as control controls. Additional strains used in this study were B6.SJL-Ptprc^{a} Pepc^{b}/BoyJ (congenic C57BL/6.CD45.1 mice from the Jackson Laboratory), C57BL/6-Tg (Tcra Tcrb)1100Mjb/J and B6.Cg-Tg(TcraTcrb)425Cbn/J (OT-I and OT-II mice from Jackson Laboratory). Mice were group-housed in individually ventilated cages and maintained under specific pathogen-free conditions. Experimental groups were sex and age-matched. Male and female littermates were used between 8 and 15 weeks of age, RNA-Seq was performed on female mice only. All animal experiments were performed in accordance with European regulation and federal law of Denmark and Germany, either approved by the Danish Animal Experiments Inspectorate, the Regierung von Oberbayern or the Landesamt für Natur-, Umwelt und Verbraucherschutz NRW.

Cell preparation

Spleens, mLNs and pLN (axillary, brachial and inguinal) were digested in RPMI containing 5% FCS, 0.5 mg/ml Collagenase IV and 15 µg/ml DNase I for 45 min at room temperature. Red blood cells in spleen and blood samples were subsequently lysed using red blood cell lysis buffer (ammonium

chloride, potassium bicarbonate, EDTA, and MiliQ water) for 3 minutes at room temperature. For the OT-II Thy1.1 adoptive transfer experiments, splenic single cell suspensions were prepared and analyzed as previously described[60].

Single cell suspensions of the intestinal LP were prepared as described previously[61]. Briefly, the intestines were flushed with HBSS supplemented with FCS (10 %), Peyer's patches were removed and epithelial cells and mucus were removed by incubating tissue in HBSS supplemented with FCS (10%) and EDTA (2 mM) 3 times each for 15 min at 37 °C with continual shaking at 450 rpm. Remaining tissue pieces were digested in R10 media (RPMI 1640 supplemented with FCS (10 %) containing DNase I grade II (30 µg/ml) and Liberase TM (58 µg/ml, Roche) for 20 min at 37 °C with a magnetic stirrer.

Lungs were perfused with PBS prior to resection. All lung lobes were cut into small pieces and digested in R5 media (RPMI 1640 supplemented with FCS (5 %) containing DNase I grade II (30 µg/ml) and Liberase TM (50 µg/ml, Roche) for 45 min at 37 °C with a magnetic stirrer.

Intestinal LP and lung cell suspensions were filtered through 100 µm cell strainers (Fisher Scientific) and leukocytes were enriched by density gradient centrifugation with 40 % / 70 % Percoll (GE Healthcare) prior to further analysis.

Flow cytometry

Single-cell suspensions were stained for multicolor analysis with the indicated fluorochrome- or biotin-conjugated antibodies after blocking with Fc block (purified anti-CD16/32). Antibodies were diluted in flow cytometry buffer (DPBS, 2% FCS) and staining was performed for 30 min on ice in the dark. LIVE/DEAD™ Fixable Near-IR Dead Cell Stain Kit (Invitrogen), Fixable Viability Dye eFluor™-780 (Invitrogen) or DRAQ7 (BioLegend) were used for determining the viability of cells. Lymphocytes from *C. rodentium* infection experiments were treated with rmIL-23 (40 ng/ml, R&D) for 3 hours at 37°C with 5% CO_2, washed and further incubated with rmIL-23 (40 ng/ml),

PMA (50 ng/ml, Sigma Aldrich), Ionomycin (750 ng/ml, Sigma Aldrich) and BD GolgiStop™ (containing monensin at 1:1000 dilution, BD) for an additional 3.5 hours at 37 °C with 5% CO_2.
For intracellular staining, cells were fixed with the Foxp3 Fixation/Permeabilization kit from eBioscience. Samples were acquired on a Fortessa X20, a LSRFortessa or a Symphony flow cytometer (BD Biosciences) using FACSDiva software (BD Biosciences) and analyzed with FlowJo software (Tree Star). The following antibodies were used: PE-Cy7/APC-Cy7 anti-mouse NK1.1 (clone PK136), PE-Cy7/BUV737/APC-Cy7 anti-mouse CD3 (clone 145-2C11 or 17A2), PE-Cy7/APC-Cy7 anti-mouse B220 (clone RA3-6B2), PE-Cy7/APC-Cy7/BUV737 anti-mouse CD19 (clone eBio1D3 or 6D5), PE-Cy7 anti-mouse CD64 (clone X54-5/7.1), APC-Cy7 anti-mouse TER119 (clone TER-119), APC/BV711/PerCP-Cy5.5 anti-mouse CD11c (clone N418/HL3), FITC/BUV661/AF700 anti-mouse MHC-II (clone M5/114.15.2), APC-Cy7/BUV737/FITC/APC-R700 anti-mouse CD11b (clone M1/70), PE/BV421 anti-mouse XCR1 (clone ZET), BV421/BV786 anti-mouse CD103 (clone M290), APC-Cy7 anti-mouse CD24 (clone M1/69), BV605 anti-mouse CD8α (clone 53-6.7), APC/PE anti-TLR3 (clone 11F8), BUV395/V500 anti-mouse CD45 (clone 30-F11), PE-CF594 anti-mouse CD172a (SIRPα) (clone P84), APC/PE-Cy7 anti-mouse ESAM (clone 1G8/ESAM), APC/PE anti-mouse IRF4 (clone 3E4), PerCP eF710 anti-mouse IRF8 (clone V3GYWCH), PE anti-mouse Clec9a (clone 7H11), FITC anti-mouse Vβ 5.1,5.2 (clone MR9-4), PerCp-Cy5.5/FITC/APC anti-mouse CD44 (clone IM7), BUV737 anti-mouse CD69 (clone H1.2F3), PE/BV421 anti-mouse CD45.2 (clone 104), Alexa Fluor® 647/PE anti-human/mouse Bcl-6 (clone K112-91), APC-Cy7 anti-mouse CD45.1 (clone A20), BUV395/BV510 anti-mouse CD4 (clone GK1.5 or RM4-5), BV786 anti-mouse IL-17A (clone TC11-18H10), FITC anti-mouse CD90.2 (clone 53-21), PerCP-Cy5.5 anti-mouse IFNγ (clone XMG1.2), PE-eF610 anti-mouse RORγt (clone BD2), PE anti-mouse IL-22 (clone 1H8BWSR), PE-Cy7 anti-mouse T-bet (clone 4B10), APC/BV421 anti-mouse Foxp3 (clone FJK-16S), APC-eF780 anti-mouse TCRβ (clone H57-597), biotin anti-mouse CXCR5 (clone L138D7), Pacific Blue™ anti-rat CD90/mouse CD90.1 (Thy-1.1) (clone OX-7), PerCP/Cyanine5.5 anti-mouse CD19 (clone 6D5), PE-eFluor™ 610/BV711 anti-mouse CD279 (PD-1) (clone J43 or 29F.1A12), and streptavidin conjugated to BUV737, BV650, or APC.

Splenic dendritic cell sorting and cDNA library preparation for RNA-seq

Splenic DC were enriched using the Dynabeads Mouse DC Enrichment kit (Invitrogen) and sorted on a BD FACS Melody to obtain cDC1 ($B220^{-}CD64^{-}CD3^{-}CD19^{-}NK1.1^{-}CD11c^{hi}MHCII^{+}XCR1^{+}$) and cDC2 ($B220^{-}CD64^{-}CD3^{-}CD19^{-}NK1.1^{-}CD11c^{hi}MHCII^{+}CD11b^{+}XCR1^{-}$). Sorted cells (2-4x$10^{4}$ per sample) were resuspended in 350 μl RNeasy Lysis Buffer (QIAGEN), and RNA was extracted using the QIAGEN RNeasy Mini kit (QIAGEN). RNA was washed, treated with DNase I (QIAGEN), and eluted per the manufacturer's instructions. RNA-seq libraries were prepared by combining the Nugen Ovation RNA-seq system with NuGEN's Ovation RNA-Seq System V2 (NuGEN Technologies). The amplified libraries were purified using AMPure beads, quantified by qPCR, and visualized on an Agilent Bioanalyzer using BioA DNA High sensitivity (Agilent). The libraries were pooled equimolarly and run on a HiSeq 2500 as single end reads of 50 nucleotide length.

RNA-sequencing data analysis

Sequencing reads were mapped to the mouse reference genome (GRCm38.85/mm10) using the STAR aligner (v2.7.6a)[62]. Alignments were guided by a Gene Transfer Format (Ensembl GTF GRCm38.101). Read count tables were normalized based on their library size factors using DESeq2 (v1.30.1)[63], and differential expression analysis was performed with a filter of log2foldChange >1 and a p-adjust value < 0.01. For selected gene signatures (cDC1 and cDC2 or $ESAM^{hi}$ and $ESAM^{lo}$ DC2s) the 100 DEGs with highest normalized count values were selected, out of which then the top 50 genes with highest absolute log2FoldChange were depicted in heatmaps. RNA-seq reads aligned to genes from the GENCODE gene annotation were counted using Ensembl's BiomaRt-v2.46.3. Heatmap visualizations were done using pheatmap v1.0.12. Downstream statistical analyses and plot generation were performed in the R environment (v4.0.5).[64] The online tool Venny 2.1 was used for the drawing of the Venn plots.[65] Package PlotMA was used for visualizing of gene expression changes from two different conditions (parameters: alpha = 0.01, type ="ashr").[66] Principal Component Analysis (PCA) plots were drawn using PCAtools 2.2.0, with removeVar=0.01.[67] Volcano plots were drawn using the

function of ggpubr 0.4.0.[68] Gene Set Enrichment Analysis was performed using Gene Ontology R package clusterProfiler 3.18.1 (category biological process) on DEGs obtained from DESeq2. The p-values were adjusted using "BH" (Benjamini-Hochberg) correction and the cutoff was 0.01.[69] GO biological process terms were ranked by GeneRatio. The gene ratio is defined as the number of genes associated with the term in DEGs divided by the number of DEGs. For KEGG enrichment, DESeq2 derived DEGs were used.[70] Enrichments with a p-value from Fisher's exact test ≤ 0.05 were considered significant.

Confocal Microscopy

Mice were sacrificed, spleens taken out, immediately washed with cold DPBS and fixed with either 4% PFA in PBS for 12 hours or 1% PFA in PBS for 24h, followed by an overnight wash with washing buffer PBS-XG (PBS + 5% FCS + 0.2% Triton X-100). Samples were embedded in warm 4% low melting agarose for sectioning. 60-100µm sections were cut using a Vibratome 1200S (Leica) and stored until use. For staining, sections were incubated with primary antibodies in 500ul washing buffer in a 24 well plate overnight at 4°C under constant agitation (120rpm), followed by at least 6 hours of washing in 5ml washing buffer. To enhance the YFP signal, a primary unlabeled anti-GFP antibody was used in the experiments based on *Clec9a.Bcl6*^{WT} and *Clec9a.Bcl6*^{KO} mice, each carrying homozygous Rosa26fl-Stop-fl-YFP alleles. This antibody was detected in a secondary antibody incubation step overnight in 500ul PBS-XG in a 24 well plate, followed by an additional washing step in 5ml washing buffer for 6 hours. The following antibodies were used: BV421 anti-mouse B220/CD45R (clone RA3-6B2), APC anti-mouse TLR3 (clone 11F8), Alexa Fluor® 488 anti-mouse CD11c (clone N418), PE-Dazzle™594 anti-mouse CD172a (SIRPα) (clone P84), unlabeled anti-GFP (polyclonal) and Alexa Fluor® 488 anti-chicken IgY (polyclonal). Sections were mounted using ProLong Gold Glass and images were acquired on a Zeiss LSM710 or a Zeiss LSM900 confocal laser microscope. Digital pictures were acquired with Zen software (Zeiss) and processed using Imaris Viewer (Oxford Instruments).

Cross-presentation assays

In vivo: Naïve $CD8^+$ T cells from OT-I donors were enriched using the Dynabeads® Untouched™ Mouse T Cells kit (Invitrogen) and stained in 1ml DPBS with CellTrace Violet dye (Invitrogen) for 10 min at 37°C. 1 x 10^6 OT-I cells were transferred into recipients one day before i.p. injection of 5 x 10^6 cells/mouse of H-$2^{\beta m1}$ MEFs expressing truncated non-secreted OVA (OVA-MEF).[17] One day after immunization, recipients were injected with FTY720 (20 µg/mouse; Cayman) in saline i.p.. Mice were sacrificed three days after immunization.

In vitro: DCs were enriched from spleen and mLN using the Dynabeads Mouse DC Enrichment kit (Invitrogen) and naïve CD8 T cells from OT-I donors were isolated using the Dynabeads Untouched Mouse T Cells kit (Invitrogen), both according to manufactures protocol. OT-I cells were stained with CellTrace Violet dye (Invitrogen) at 1:1000 in PBS for 10 min at 37°C. Enriched DCs from both mLN and spleen were incubated with OVA (InvivoGen, EndoFit) at a concentration of 250mg/ml in culture media (RPMI 1640 supplemented with 10 % FCS, 55 µM β-mercaptoethanol and Penicillin-Streptomycin-Glutamin 100x (Gibco)) for 2h at 37°C and washed twice. DCs for negative control were not incubated with OVA. The frequency of cDC1s in each sample was determined using flow cytometry, and 670 cDC1s were plated in a cell culture treated 96-well U bottom plate with 0.2x10^6 OT-I cells in culture media supplemented with 1ug/ml LPS. For the positive control, 0.2x10^6 OT-I cells were stimulated with 10ug/ml aCD3 (eBioscience, clone 17A2) (plate bound) and 1 ug/ml aCD28 (eBioscience, clone 37.51). Flowcytometry-based analysis was carried out after incubation for 65h at 37°C with 5% CO_2.

Induction of Tfh cells and antibody responses *in vivo*

For adoptive transfer experiments into *CD11c.Bcl6^{KO}* or control hosts, naïve $CD4^+$ T cells were enriched from homozygous TCR-transgenic OT-II (CD45.1/.2) donors using the Dynabeads Untouched™ Mouse CD4 Cells kit (Invitrogen). 1 x 10^5 OT-II cells were transferred intravenously (i.v.) and one day later, recipients were immunized i.p. with ovalbumin grade V (OVA, 0.5 mg, Sigma Aldrich) together with poly(I:C) (100 µg, Sigma-Aldrich). Controls received PBS alone and mice were sacrificed three days after immunization. For adoptive transfer experiments into *Clec9a.Bcl6^{WT}* or *Clec9a.Bcl6^{KO}* hosts, naïve $CD8^-CD19^-CD44^{int/low}CD62L^{hi}CD25^-$ $CD4^+$ T cells were

sorted from heterozygous OT-II (CD45.1/2) donors on BD FACSAria III or Fusion cell sorters. $5x10^5$ OT-II cells were injected i.v., and one day later, recipient mice were immunized i.p. with a 1:1 mixture of 50 µg NP_{17}-OVA ((#N-5051-10-BS Biosearch Technologies/BioCat) in PBS and Imject Alum (Thermo Fisher). For assessment of endogenous Tfh and Tfr cell responses, *Clec9a.Bcl6*^{CONTROL} or *Clec9a.Bcl6*^{KO} mice were immunized i.p. with 50µg NP_{32}-KLH (#N-5060-5, Biosearch Technologies/BioCat) in PBS and Imject Alum (Thermo Fisher). Spleens were dissected and analyzed by flow cytometry on day 14. In independent NP_{32}-KLH/alum-immunized cohorts, blood samples were collected on days 7, 14, 21, and 28 using Microvette 200 Serum Gel CAT tubes (#20.1291, Sarstedt) and NP-specific serum antibody levels were determined by ELISA.

ELISA

To measure NP-specific serum IgG1 and total IgG, half-area radio-immunoassay plates (#3690, Corning) were coated with 25 µl of 10 µg/ml NP-BSA in PBS (N-5050XL-10-BS with loading ratio of 2 or N-5050H-10-BS with loading ratio of 36, both Biosearch Technologies/BioCat) overnight at 4 °C. The next day, plates were washed four times with PBS + 0,005 % Tween20 and then blocked with 70 µl PBS + 2 % BSA for 2h at RT. After four washing steps, serial dilutions of serum from immunized mice were added to the plate and incubated on a plate shaker for 2h at RT. Pooled sera from day 28-immunized mice were used as standard. Next, plates were washed four times and 25 µl of a 1:500 dilution of the respective detection antibody (goat anti-mouse IgG(H+L)-alkaline phosphatase (AP) conjugate (#SBA-1036-04) or goat anti-mouse IgG1-AP (#SBA-1071-04), all Southern Biotech/Biozol) was added to each well and incubated for 45 min while shaking. Plates were washed four times and then incubated with 70 µl of Alkaline Phosphatase Solution (#P7998-100ML, Sigma Aldrich) for 20 min. Plates were read for absorbance at 405 nm (TriStar plate reader). Resulting data were plotted as concentration (x axis) versus OD (OD, y axis) in Excel, then fit to a sigmoidal 4 parameter logistic (4PL) model by utilizing the Four Parameter Logistic (4PL) Curve Calculator (AAT Bioquest Inc.). The sigmoidal 4PL equations were then used to calculate the concentration of individual samples. Values are expressed as arbitrary units (AU).

***Citrobacter rodentium* infection**

The *C. rodentium* strain DBS100 (ATCC 51459; American Type Culture Collection) was used as described[71] with some amendments. Briefly, *C. rodentium* cultures were grown in Luria-Bertani (LB) medium to an OD_{600} of 1-1.5. Mice were orally inoculated with LB broth or $2x10^9$ CFU *C. rodentium*, and their weight was monitored daily. Fecal samples were collected on indicated days post infection, serially diluted in PBS and plated on Brilliance™ E. coli/coliform Agar (Thermo Fisher). *C. rodentium* colonies, from at least three dilutions per sample, were enumerated and normalized to weight of feces.

For histopathology, 0.5 cm of the distal colon was immediately placed in 10% formalin and processed by the DTU Histology Core for hematoxylin and eosin (H&E) staining. Images were acquired on a Pannoramic MIDI II scanner (3DHISTECH) and visualized with CaseViewer software 2.4 (3DHISTECH). The severity of the infection was assessed in a blinded manner.

Statistical Analysis

Statistical analyses were performed with Graphpad Prism 9.0 (Graphpad Software).

Supplementary Materials

Supplementary Figure 1: cDC-gating strategies accompanying Figure 1 and 2

Supplementary Figure 2: Phenotype and abundance of lung and blood cDC lacking Bcl6

Supplementary Figure 3: Expression levels of CD11b in cDC1 and cDC2 across genotypes and organs

Supplementary Figure 4: In vitro cross-presentation

Supplementary Figure 5: Expression of IL-6 pathway genes in cDC1 from *XCR1.Bcl6*^{KO} versus control mice

Supplementary Figure 6: Quantification of spleen cDC in *Clec9a.Bcl6^{KO}* miceSupplementary Figure 7: CD11c- versus Clec9a.YFP-based cDC-gating strategies

Supplementary Figure 8: Effect of DC-specific Bcl6 deficiency on Tfh cell and antibody responses

Supplementary Figure 9: Intracellular Foxp3 and cytokine staining of colonic CD4^{+} T cells from *Citrobacter rodentium*-infected mice

Supplementary Figure 10: Colonic CD4^{+} T cell subsets in day 9 *Citrobacter rodentium* infected *Clec9a.Bcl6^{KO}* and control mice

Supplementary Table 1: Expression levels of top 50 DEGs between control cDC1 and control cDC2

Supplementary Table 2: DEGs between control and *XCR.Bcl6^{KO}* cDC1 and control and *CD11c.Bcl6^{KO}* cDC2

Supplementary Table 3: Expression levels of top 50 DEGs between ESAM^{hi} and ESAM^{lo} cDC2

References

1. Guilliams, M. *et al.* Dendritic cells, monocytes and macrophages: a unified nomenclature based on ontogeny. *Nature Reviews Immunology* **14**, 571–578 (2014).
2. Steinman, R. M. the Dendritic Cell System. *Annual Review of Immunology* **9**, 271–296 (1991).
3. Durai, V. & Murphy, K. M. Functions of Murine Dendritic Cells. *Immunity* **45**, 719–736 (2016).
4. Allenspach, E. J., Lemos, M. P., Porrett, P. M., Turka, L. A. & Laufer, T. M. Migratory and Lymphoid-Resident Dendritic Cells Cooperate to Efficiently Prime Naive CD4 T cells. *Immunity* **29**, 795–806 (2008).
5. Lewis, S. M., Williams, A. & Eisenbarth, S. C. Structure and function of the immune system in the spleen. *Science Immunology* **4**, (2019).

6. Eisenbarth, S. C. Dendritic cell subsets in T cell programming: location dictates function. *Nature Reviews Immunology* **19**, (2018).
7. Calabro, S. *et al.* Differential Intrasplenic Migration of Dendritic Cell Subsets Tailors Adaptive Immunity. *Cell Reports* **16**, 2472–2485 (2016).
8. Idoyaga, J., Suda, N., Suda, K., Park, C. G. & Steinman, R. M. Antibody to Langerin/CD207 localizes large numbers of CD8α + dendritic cells to the marginal zone of mouse spleen. *Proceedings of the National Academy of Sciences of the United States of America* **106**, 1524–1529 (2009).
9. Sichien, D. *et al.* IRF8 Transcription Factor Controls Survival and Function of Terminally Differentiated Conventional and Plasmacytoid Dendritic Cells, Respectively. *Immunity* **45**, 626–640 (2016).
10. Schiavoni, G. *et al.* ICSBP is essential for the development of mouse type I interferon-producing cells and for the generation and activation of CD8α+ dendritic cells. *Journal of Experimental Medicine* **196**, 1415–1425 (2002).
11. Hildner, K. *et al.* Batf3 deficiency reveals a critical role for CD8alpha+ dendritic cells in cytotoxic T cell immunity. *Science* **322**, 1097–1100 (2008).
12. Kashiwada, M., Pham, N. L. L., Pewe, L. L., Harty, J. T. & Rothman, P. B. NFIL3/E4BP4 is a key transcription factor for CD8α+ dendritic cell development. *Blood* **117**, 6193–6197 (2011).
13. Bagadia, P. *et al.* An Nfil3–Zeb2–Id2 pathway imposes Irf8 enhancer switching during cDC1 development. *Nature Immunology* **20**, 1174–1185 (2019).
14. Hacker, C. *et al.* Transcriptional profiling identifies Id2 function in dendritic cell development. *Nature Immunology* **4**, 380–386 (2003).
15. Cerovic, V. *et al.* Lymph-borne CD8α+ dendritic cells are uniquely able to cross-prime CD8+ T cells with antigen acquired from intestinal epithelial cells. *Mucosal Immunology* **8**, 38–48 (2015).

16. Joeris, T. *et al.* Intestinal cDC1 drive cross-tolerance to epithelial-derived antigen via induction of FoxP3+CD8+ Tregs. *Science immunology* **6**, (2021).
17. Sancho, D. *et al.* Identification of a dendritic cell receptor that couples sensing of necrosis to immunity. *Nature* **458**, 899–903 (2009).
18. Ahrens, S. *et al.* F-actin is an evolutionarily conserved damage-associated molecular pattern recognized by DNGR-1, a receptor for dead cells. *Immunity* **36**, 635–45 (2012).
19. Zhang, J.-G. *et al.* The dendritic cell receptor Clec9A binds damaged cells via exposed actin filaments. *Immunity* **36**, 646–57 (2012).
20. Watchmaker, P. B. *et al.* Comparative transcriptional and functional profiling defines conserved programs of intestinal DC differentiation in humans and mice. *Nature immunology* **15**, 98–108 (2014).
21. Tussiwand, R. *et al.* Klf4 Expression in Conventional Dendritic Cells Is Required for T Helper 2 Cell Responses. *Immunity* **42**, 916–928 (2015).
22. Satpathy, A. T. *et al.* Notch2-dependent classical dendritic cells orchestrate intestinal immunity to attaching-and-effacing bacterial pathogens. *Nat Immunol* **14**, 937–948 (2013).
23. Persson, E. K. *et al.* IRF4 transcription-factor-dependent CD103(+)CD11b(+) dendritic cells drive mucosal T helper 17 cell differentiation. *Immunity* **38**, 958–69 (2013).
24. Williams, J. W. *et al.* Transcription factor IRF4 drives dendritic cells to promote Th2 differentiation. *Nat Commun* **4**, 2990 (2013).
25. Scott, C. L. *et al.* The transcription factor Zeb2 regulates development of conventional and plasmacytoid DCs by repressing Id2. *The Journal of Experimental Medicine* jem.20151715 (2016) doi:10.1084/jem.20151715.

26. Ichikawa, E. *et al.* Defective development of splenic and epidermal CD4+ dendritic cells in mice deficient for IFN regulatory factor-2. *Proceedings of the National Academy of Sciences of the United States of America* **101**, 3909–14 (2004).
27. Wu, L. *et al.* RelB is essential for the development of myeloid-related CD8alpha- dendritic cells but not of lymphoid-related CD8alpha+ dendritic cells. *Immunity* **9**, 839–47 (1998).
28. Lewis, K. L. *et al.* Notch2 receptor signaling controls functional differentiation of dendritic cells in the spleen and intestine. *Immunity* **35**, 780–791 (2011).
29. Briseño, C. G. *et al.* Notch2-dependent DC2s mediate splenic germinal center responses. *Proceedings of the National Academy of Sciences of the United States of America* **115**, 10726–10731 (2018).
30. Fasnacht, N. *et al.* Specific fibroblastic niches in secondary lymphoid organs orchestrate distinct Notch-regulated immune responses. *Journal of Experimental Medicine* **211**, 2265–2279 (2014).
31. Caton, M. L., Smith-Raska, M. R. & Reizis, B. Notch–RBP-J signaling controls the homeostasis of CD8 − dendritic cells in the spleen . *The Journal of Experimental Medicine* **204**, 1653–1664 (2007).
32. Lu, E., Dang, E. V., McDonald, J. G. & Cyster, J. G. Distinct oxysterol requirements for positioning naïve and activated dendritic cells in the spleen. *Science Immunology* **2**, eaal5237 (2017).
33. Choi, J. & Crotty, S. Bcl6-Mediated Transcriptional Regulation of Follicular Helper T cells (TFH). *Trends in Immunology* **42**, 336–349 (2021).
34. Ohtsuka, H. *et al.* Bcl6 Is Required for the Development of Mouse CD4+ and CD8 + Dendritic Cells. *The Journal of Immunology* **186**, 255–263 (2011).
35. Bagadia, P. *et al.* Bcl6 -Independent In Vivo Development of Functional Type 1 Classical Dendritic Cells Supporting Tumor Rejection . *The Journal of Immunology* ji1901010 (2021) doi:10.4049/jimmunol.1901010.

36. Schraml, B. U. *et al.* Genetic tracing via DNGR-1 expression history defines dendritic cells as a hematopoietic lineage. *Cell* **154**, 843–858 (2013).
37. Lau, C. M. *et al.* Leukemia-associated activating mutation of Flt3 expands dendritic cells and alters T cell responses. *Journal of Experimental Medicine* **213**, 415–431 (2016).
38. Baumjohann, D., Okada, T. & Ansel, K. M. Cutting Edge: Distinct Waves of BCL6 Expression during T Follicular Helper Cell Development. *The Journal of Immunology* **187**, 2089–2092 (2011).
39. Goenka, R. *et al.* Cutting Edge: Dendritic Cell-Restricted Antigen Presentation Initiates the Follicular Helper T Cell Program but Cannot Complete Ultimate Effector Differentiation. *The Journal of Immunology* **187**, 1091–1095 (2011).
40. Baumjohann, D. *et al.* Persistent Antigen and Germinal Center B Cells Sustain T Follicular Helper Cell Responses and Phenotype. *Immunity* **38**, 596–605 (2013).
41. Ribeiro, F., Perucha, E. & Graca, L. T follicular cells: The regulators of germinal center homeostasis. *Immunol Lett* **244**, 1–11 (2022).
42. Wing, J. B., Lim, E. L. & Sakaguchi, S. Control of foreign Ag-specific Ab responses by Treg and Tfr. *Immunol Rev* **296**, 104–119 (2020).
43. Zhang, S. *et al.* Type 1 conventional dendritic cell fate and function are controlled by DC-SCRIPT. *Science immunology* **6**, (2021).
44. Zhang, T. T. *et al.* Dynamic expression of BCl6 in murine conventional dendritic cells during in vivo development and activation. *PLoS ONE* **9**, 1–12 (2014).
45. Durai, V. *et al.* Cryptic activation of an Irf8 enhancer governs cDC1 fate specification. *Nature Immunology* **20**, 1161–1173 (2019).
46. Grajales-Reyes, G. E. *et al.* Batf3 maintains autoactivation of Irf8 for commitment of a CD8α+ conventional DC clonogenic progenitor. *Nature Immunology* **16**, 708–717 (2015).

47. Seillet, C. *et al.* Nfil3 is required for the development of all innate lymphoid cell subsets. *The Journal of experimental medicine* **211**, 1733–40 (2014).
48. Kusunoki, T. *et al.* TH2 dominance and defective development of a CD8+ dendritic cell subset in Id2-deficient mice. *Journal of Allergy and Clinical Immunology* **111**, 136–142 (2003).
49. Dudziak, D. *et al.* Differential antigen processing by dendritic cell subsets in vivo. *Science (New York, N.Y.)* **315**, 107–11 (2007).
50. Gatto, D. *et al.* The chemotactic receptor EBI2 regulates the homeostasis, localization and immunological function of splenic dendritic cells. *Nature Immunology* **14**, 446–453 (2013).
51. Yi, T. & Cyster, J. G. EBI2-mediated bridging channel positioning supports splenic dendritic cell homeostasis and particulate antigen capture. *eLife* **2**, e00757 (2013).
52. Huang, C. *et al.* The BCL6 RD2 Domain Governs Commitment of Activated B Cells to Form Germinal Centers. *Cell Reports* **8**, 1497–1508 (2014).
53. Crotty, S., Johnston, R. J. & Schoenberger, S. P. Effectors and memories: Bcl-6 and Blimp-1 in T and B lymphocyte differentiation. *Nat Immunol* **11**, 114–120 (2010).
54. Choi, J. & Crotty, S. Bcl6-Mediated Transcriptional Regulation of Follicular Helper T cells (TFH). *Trends in Immunology* **42**, 336–349 (2021).
55. Baumjohann, D. & Fazilleau, N. Antigen-dependent multistep differentiation of T follicular helper cells and its role in SARS-CoV-2 infection and vaccination. *Eur J Immunol* **51**, 1325–1333 (2021).
56. Schlitzer, A. *et al.* IRF4 transcription factor-dependent CD11b+ dendritic cells in human and mouse control mucosal IL-17 cytokine responses. *Immunity* **38**, 970–83 (2013).
57. Kedmi, R. *et al.* A RORγt+ cell instructs gut microbiota-specific Treg cell differentiation. *Nature* (2022) doi:10.1038/s41586-022-05089-y.
58. Wohn, C. *et al.* Absence of MHC class II on cDC1 dendritic cells triggers fatal autoimmunity to a cross-presented self-antigen. *Science immunology* **5**, (2020).

59. Hollister, K. *et al.* Insights into the Role of Bcl6 in Follicular Th Cells Using a New Conditional Mutant Mouse Model. *The Journal of Immunology* **191**, 3705–3711 (2013).
60. Baumjohann, D. & Ansel, K. M. Tracking Early T Follicular Helper Cell Differentiation In Vivo. in *Methods in molecular biology* vol. 1291 27–38 (2015).
61. Johansson-Lindbom, B. *et al.* Functional specialization of gut CD103 + dendritic cells in the regulation of tissue-selective T cell homing . *The Journal of Experimental Medicine* **202**, 1063–1073 (2005).
62. Dobin, A. *et al.* STAR: Ultrafast universal RNA-seq aligner. *Bioinformatics* **29**, 15–21 (2013).
63. Love, M. I., Huber, W. & Anders, S. Moderated estimation of fold change and dispersion for RNA-seq data with DESeq2. *Genome Biology* **15**, (2014).
64. R Core Team (2020). R: A language and environment for statistical computing. R Foundation for Statistical Computing, Vienna, Austria. Preprint at (2020).
65. Oliveros, J. C. Venny. An Interactive Tool for Comparing Lists with Venn's Diagrams.
66. Stephens, M. False discovery rates: A new deal. *Biostatistics* **18**, 275–294 (2017).
67. Blighe, K. and A. L. PCAtools: everything Principal Components Analysis.https://github.com/kevinblighe/PCAtools. Preprint at (2019).
68. Alboukadel Kassambara. ggpubr:'ggplot2' Based Publication Ready Plots. Preprint at (2020).
69. Yu, G., Wang, L.-G., Han, Y. & He, Q.-Y. clusterProfiler: an R Package for Comparing Biological Themes Among Gene Clusters. *OMICS: A Journal of Integrative Biology* **16**, (2012).
70. Qiu, Y.-Q. KEGG Pathway Database. in *Encyclopedia of Systems Biology* (eds. Dubitzky, W., Wolkenhauer, O., Cho, K.-H. & Yokota, H.) 1068–1069 (Springer New York, 2013). doi:10.1007/978-1-4419-9863-7_472.
71. Rizk, J. *et al.* The cIAP ubiquitin ligases sustain type 3 γδ T and innate lymphoid cells during aging to allow normal cutaneous and mucosal responses. *bioRxiv* (2022) doi:10.1101/2020.05.14.094334.

Acknowledgements

We thank Katrine Fog Starup, Julien Vandamme, Frank Dahlström, and Jennifer-Christin Becker for excellent technical support, the Lahl, Agace, Bekiaris, and Baumjohann laboratories for fruitful discussions, and Prof Allan Mowat for intellectual input and manuscript editing. *Bcl6*$^{fl/fl}$ mice were kindly gifted by Alexander Dent and the OVA-MEF line was from Caetano Reis e Sousa. H&E sections were processed by Susanne Primdahl and histology data was generated using research infrastructure at DTU National Food Institute, including FOODHAY (Food and Health Open Innovation Laboratory, Danish Roadmap for Research Infrastructure). We acknowledge the BMC Core Facility Flow Cytometry of LMU Munich for providing equipment and the Core Facility of the Medical Faculty at the University of Bonn for providing support and instrumentation funded by the Deutsche Forschungsgemeinschaft (DFG, German Research Foundation) (387333827, 216372545, 216372401, 387335189).

Funding

China Scholarship Council fellowship (HX)
Lundbeck Foundation Fellowship R215-2015-4100 (KL)
Ragnar Söderberg Foundation Fellowship in Medicine (KL)
Vetenskapsrådet 2020-01977 (KL)
Cancerfonden 21 1826 Pj (KL)
Novo Nordisk Foundation 18038 (KL)
Crafoord Foundation (KL)
European Research Council ERC-2016-STG-715182 (BS)
Deutsche Forschungsgemeinschaft (DFG, German Research Foundation) Emmy Noether grant Schr 1444/1-1, Project-ID 360372040 – SFB 1335 (project 8) and 322359157-FOR2599-A03 (BS)
Deutsche Forschungsgemeinschaft (DFG, German Research Foundation) Emmy Noether Programme BA 5132/1-1 and BA 5132/1-2 (252623821), SFB 1054 Project B12 (210592381) and Germany's Excellence Strategy EXC2151 (390873048) (DB).

Author Contributions:

Conceptualization: DB, KL

Methodology: HX, IU, JH, HN, LB, IK, SH, UM, LZ, AS, FP, BS, DB, KL

Investigation: HX, IU, JH, HN, LB, IK, SH, UM, LZ, BS, DB, KL

Visualization: HX, IU, UM, DB, KL

Funding acquisition: HX, DB, BS, KL

Project administration: KL

Supervision: FP, AS, BS, DB, KL

Writing – original draft: KL

Writing – review & editing: IU, BS, DB, KL

Competing Interests

The authors declare that they have no competing interests.

Data Availability

Raw RNA-sequencing data files are accessible through the NCBI SRA database under the accession number PRJNA834905.

Figures:

Fig. 1: Phenotype and abundance of lymphoid tissue resident cDC lacking Bcl6

A. Left: Splenic XCR1^{+} and XCR1^{-}CD11b^{+} DC subsets in control (black), *XCR1.Bcl6^{KO}* (red), and *CD11c.Bcl6^{KO}* (orange) mice. Plots show representative staining profiles of gated live, single lineage^{-} (CD3, CD19, CD64, B220, NK1.1), MHCII^{+}, CD11c^{hi} splenocytes. Right: Absolute numbers of splenic XCR1^{+} and XCR1^{-}CD11b^{+} DC from control, *XCR1.Bcl6^{KO}*, and *CD11c.Bcl6^{KO}* mice. Statistical analysis by one-way ANOVA. * P<0.01 and ** P<0.001. Data points represent values from individual mice pooled from 8-9 experiments and lines represent the medians.

B. Left: Flow cytometry plots showing resident XCR1$^+$ and XCR1$^-$CD11b$^+$ DC subsets in the pLNs and mLNs of control, *XCR1.Bcl6^{KO}*, and *CD11c.Bcl6^{KO}* mice. Plots show representative staining profiles of gated single live, CD45$^+$, lineage$^-$ (CD3, CD19, CD64, B220, NK1.1), CD11c^{hi}MHCII^{int} resident DC. Right: Absolute numbers of resident cDC subsets in the pLN and mLN of control, *XCR1.Bcl6^{KO}*, and *CD11c.Bcl6^{KO}* mice. Statistical analysis by one-way ANOVA. * P<0.05. Data points represent values from individual mice pooled from at least four experiments and lines represent the medians.

Fig. 2: Phenotype and abundance of migratory cDC subsets lacking Bcl6

A. Left: Flow cytometry plots showing migratory XCR1$^+$ and XCR1$^-$CD11b$^+$ DC subsets in the pLN (top) and mLN (middle) of control (black), *XCR1.Bcl6^{KO}* (red), and *CD11c.Bcl6^{KO}* (orange) mice. mLN XCR1$^-$ DC are further sub-divided into CD103$^+$ and CD103$^-$ (bottom). Plots show representative staining profiles of live single, CD45$^+$, lineage$^-$ (CD3, CD19, CD64, B220, NK1.1), CD11c^{int}MHCII^{hi} migratory DC. Right: Absolute numbers of migratory cDC subsets from pLN and mLN of control, *XCR1.Bcl6^{KO}*, and *CD11c.Bcl6^{KO}* mice. Statistical analysis by one-way ANOVA. * P<0.05, ** P<0.01, *** P<0.001 and **** P<0.0001. Data points represent values from individual mice pooled from at least four experiments and lines represent the medians.

B. Left: Flow cytometry plots showing SILP XCR1$^+$ and XCR1$^-$CD11b$^+$ DC subsets from control, *XCR1.Bcl6^{KO}*, and *CD11c.Bcl6^{KO}* mice. Plots show representative staining profiles of live, CD45$^+$, lineage$^-$ (CD3, CD19, CD64, B220, NK1.1), MHCII$^+$, CD11c^{hi} gated single cells.
Right: Absolute numbers of XCR1$^+$ and XCR1$^-$CD11b$^+$ DC subsets from control, *XCR1.Bcl6^{KO}*, and *CD11c.Bcl6^{KO}* mice. Statistical analysis was performed by one-way ANOVA.* P<0.05 and ** P<0.01. Data points represent values from individual mice pooled from three experiments and lines represent the medians.

Fig. 3: Lineage identity of splenic Bcl6-deficient cDC subsets

A. Principal component analysis (PCA) plot of gene expression data obtained from bulk RNA-seq using DESeq2. Color coded icons show cDC1 and cDC2 from the spleen of control, *XCR1.Bcl6^{KO}*, and *XCR1.Bcl6^{KO}* mice. Three replicates were included in each group.

B. Heatmap of selected highly expressed cDC1 or cDC2 associated genes in all RNA-Seq samples (50 most differentially expressed genes between cDC1 and cDC2 chosen from the 100 genes with

highest expression level among total differentially expressed genes (fold change ≥ 2, padj: 0.01) in control samples). The color scale represents the row Z score.

C. Volcano plots showing the global transcriptional differences between splenic cDC2 and cDC1 in control (left), *XCR1.Bcl6*^{KO} (middle) and *CD11c.Bcl6*^{KO} mice (right). Each circle represents one gene. The log2FoldChange (LFC) is represented on the x-axis. The y-axis shows the –(log10 of the p adjust value). A padj value of 0.01 and an absolute LFC of 1 are indicated by dashed lines. The upregulated or downregulated genes are shown in red or blue dots respectively, and the top ranked gene symbols with the lowest padj value were annotated in the plot.

D. VENN diagram showing significantly elevated differentially expressed genes (DEGs) (|Log2foldchange|≥1 and padj<0.01) between *XCR1.Bcl6*^{KO} cDC1 (red) and control cDC1 (blue), and between *CD11c.Bcl6*^{KO} cDC2 (orange) and control cDC2 (green).

Fig. 4: Phenotype and cross-presentation abilities by cDC1 deficient in Bcl6

A. Flow cytometric analysis of cDC1 in spleen of control and *XCR1.Bcl6*^{KO} mice. Representative histograms show indicated protein expression by control (black) and *XCR1.Bcl6*^{KO} (red) cDC1, with FMO staining shown in grey and control cDC2 shown as a dashed line. Dot plots show FMO-subtracted MFI values. Pre-gating on cDC1 and cDC2 was performed as in 1A. Histograms are representative of three independent experiments with 3 mice each and MFI plots show 2 out of 3 experiments. * P<0.05, ** P<0.01

B. Representative flow cytometry plots showing CTV dilution and CD44 expression on OT-I cells (gated on live, $CD3^{+}CD8^{+}CD45.1^{+}$ single cells) in the spleen (top) and mLN (bottom) of control and *XCR1.Bcl6*^{KO} recipient mice three days after i.p. immunization with heat-shocked OVA-MEFs. Data are representative of three independent experiments with 2-5 mice each.

C. Total number of OT I cells in the spleen (right) and mLN (left) of immunized control and *XCR1.Bcl6*^{KO} mice. Data are pooled from three independent experiments. Each dot represents one mouse and lines represent the medians. Statistical analysis using Mann-Whitney test, *p<0.05.

A. **Fig. 5: Differentially expressed genes in Bcl6-deficient splenic cDC1** Gene ontology (GO) term enrichment analysis of differentially expressed genes (DEGs) in *XCR1.Bcl6*^{KO} and control cDC1. The

p value calculated from GO term enrichment analysis is represented on the x-axis and the y-axis shows the GO Biological Process (BP) terms.

B. KEGG (Kyoto Encyclopedia of Genes and Genomes) term enrichment analysis of DEGs in *XCR1.Bcl6*^{KO} vs control cDC1. The GeneRatio value calculated from KEGG term enrichment analysis is represented on the x-axis and the y-axis shows the KEGG enriched terms.

C. Heatmap of all genes contributing to the enriched KEGG pathways depicted in B. The color scale represents the row Z score.

D. IL-6 levels in the serum of *XCR1.Bcl6*^{KO} vs control mice injected intraperitoneally with poly(I:C) 2 hours before analysis. Data is pooled from 6 experiments with 1-6 mice each (2 experiments without untreated controls). * P<0.05, ** P<0.01, *** P<0.001.

Fig. 6: Phenotype and gene expression profiles of splenic Bcl6-deficient cDC2

A. Representative flow cytometric analysis of cDC2 in the spleen of control and *CD11c.Bcl6*^{KO} mice, showing expression of CD11c vs MHCII (top panels) and XCR1 vs CD11b (lower panels) by live, lineage^{-} (CD3, CD19, CD64, B220, NK1.1), CD11c^{+} single cell-gated splenocytes. Data are representative of at least 8 independent experiments with 1 – 3 mice each. Reported MFI levels of MHCII are raw values and average deviation from 3 experiments with 3 mice each.

B. Representative flow cytometric analysis of ESAM^{hi} and ESAM^{lo} cDC2 in the spleen of control and *CD11c.Bcl6*^{KO} mice. Cells were pre-gated as XCR1^{-}CD11b^{+} cDC2 from live, lineage^{-} (CD3, CD19, CD64, B220, NK1.1), CD11c^{+}, MHCII^{+} single cells. Data are representative of three independent experiments with 1 – 3 mice each.

C. Representative flow cytometric analysis of cDC2 in the spleen of control and *Clec9a.Bcl6*^{KO} mice, showing expression of CD11c vs MHCII (top panels) and XCR1 vs CD11b (lower panels, gated on CD11c^{+}, MHCII^{+}) by live, lineage^{-} (CD3, CD19, CD64, B220, NK1.1) single cell-gated splenocytes. Data are representative of two independent experiments with 3 mice each.

D. Representative flow cytometric analysis of ESAM^{hi} and ESAM^{lo} cDC2 in the spleen of control and *Clec9a.Bcl6*^{KO} mice. Cells were pre-gated as XCR1^{-}CD11b^{+} cDC2 from live, lineage^{-} (CD3, CD19, CD64, B220, NK1.1), CD11c^{+}, MHCII^{+} single cells (top). Data are representative of two independent experiments with 3 mice each.

E. Same data as in D, but pre-gated on YFP^{+} instead of CD11c^{+} (see suppl. Fig. 4 for full gating strategy).

F. Representative flow cytometric analysis of expression of CD11c, 33D1, CD4, CD11b and IRF4 by splenic XCR1^{-}CD11b^{+} cDC2 from control (ESAM^{hi}: black, ESAM^{lo}: blue) or *CD11c.Bcl6^{KO}* mice (orange). FMO controls are depicted in gray. Gates correspond to those depicted in Fig. 6B. Results are representative of at least two (CD11c) or three (all others) independent experiments with 3 mice each.

Fig. 7: Gene signature comparisons between ESAM and ESAM cDC2 with Bcl6-deficient cDC2

A. Gene set enrichment plots following *CD11c.Bcl6^{KO}* vs control cDC2 in an ESAM^{hi} cDC2 related gene set (top) vs an ESAM^{lo} cDC2 related gene set (bottom) (ESAM^{hi} and ESAM^{lo} gene sets derived from GSE76132). NES = normalized enrichment score. FDR q-value: 0.0.
B. The top 50 genes associated with spleen ESAM^{hi} cDC2 (left) or ESAM^{lo} cDC2 (right) were derived from GSE76132. Heatmaps show the expression of these genes in the RNA-Seq analysis of cDC2 from control and *CD11c.Bcl6^{KO}* spleen. The color scale represents the row Z score (Expression Z-scale).

Fig. 8: Impact of Bcl6 deficiency in splenic cDC on Tfh cell and antibody responses

A. Confocal microscopy of spleens from *CD11c.Bcl6^{KO}* and control mice showing expression of TLR3 (grey), CD11c (green), Sirpα (red) and B220 (blue). Scale bar=50μm. Orange arrows indicate marginal zone bridging channels. The images shown are from one out of four (*CD11c.Bcl6^{KO}*) or three (control) replicates derived from individual mice.
B. Confocal microscopy of spleens from *Clec9a.Bcl6^{WT} and Clec9a.Bcl6^{KO} mice, each carrying homozygous Rosa26$^{fl\text{-}Stop\text{-}fl\text{-}YFP}$ alleles,* showing expression of TLR3 (grey), YFP (green, Clec9A reporter), CD11c (red) and B220 (blue). Scale bar=50μm. Single channel figures are derived from the areas in the yellow boxes. The images shown are from one out of four replicates derived from individual mice.
C. Experimental design.
D. Representative flow cytometric analysis of splenic OT-II cells transferred into *Clec9a.Bcl6^{CONTROL}* and *Clec9a.Bcl6^{KO}* recipients 7 days after i.p. immunization with OVA/alum. Tfh cells were gated as CXCR5^{+}PD-1^{+} cells among live CD4^{+} CD19^{-} lymphocytes. Statistical analysis was performed by

Mann-Whitney test, ** P<0.01. Each symbol represents one biological replicate (n=4-5), lines represent the median. Data are representative of two independent experiments.

E. Experimental design.

F. Total cellularity and number of $CD4^+Foxp3^-$ and $CD4^+Foxp3^+$ cells in *Clec9a.Bcl6^{KO}* and control mice 14 days after i.p. injection with NP-KLH and alum adjuvant. Data is pooled from two independent experiments, each with 4-5 mice per group.

G. Representative flow cytometric analysis of $Foxp3^-$ (left) and $Foxp3^+$ (right) $CD4^+$ T cell-gated splenocytes 14 days post NP-KLH/alum i.p. immunization of *Clec9a.Bcl6^{KO}* and control mice. $Foxp3^-$: Tfh cells are gated as $CXCR5^{int}PD\text{-}1^{int}$ and GC Tfh cells are gated as $CXCR5^{hi}PD\text{-}1^{hi}$. $Foxp3^+$: Tfr cells are gated as $CXCR5^{hi}PD\text{-}1^{hi}$. Data is pooled from two independent experiments, each with 4-5 mice per group.

H. Quantification of data shown in G.

I. Experimental design.

J. NP-specific total IgG in the serum from NP-KLH and alum immunized *Clec9a.Bcl6^{KO}* and control mice at indicated time-points as determined by ELISA for low (NP36)- and high (NP2)-affinity antibody. Data are representative of two independent experiments with 4-5 mice each. Two-way ANOVA with Bonferroni post-hoc, * P<0.05, ** P<0.01.

Fig. 9: *Citrobacter rodentium* infection in mice with Bcl6 deletion in cDC

A. Left: Flow cytometry plots showing cLP $XCR1^+$ and $XCR1^-CD11b^+$ DC subsets gated on all DC (live, $CD45^+$, $lineage^-$ (CD3, CD19, CD64, B220, NK1.1), $MHCII^+$, $CD11c^{hi}$ single cells. Right: $XCR1^-$ DC are further sub-divided into $CD103^+$ and $CD103^-$ cDC2s from control and *CD11c.Bcl6^{KO}* mice.

B. Absolute numbers (top) and proportions (bottom) of cLP $XCR1^+$, $XCR1^-CD103^+CD11b^+$ and $XCR1^-CD103^-CD11b^+$ DC subsets from control and *CD11c.Bcl6^{KO}* mice. Data points represent values from individual mice pooled from 3 experiments and lines represent the medians. Statistical analysis using Mann-Whitney test, ** P<0.01 and *** P<0.001.

C. Percentage of weight loss of mock and *C. rodentium* infected control and *CD11c.Bcl6^{KO}* mice. Each symbol represents the mean weight loss of all mice within the group at the indicated time point post infection versus their starting weight and error bars represent SD; statistical analysis using two-way ANOVA (and Tukey's multiple comparison test) with Geisser-Greenhouse correction, *P < 0.05 and **P < 0.01 (top left). Colon lengths in mock and infected mice at 9 or 21 days post

inoculation; statistical analysis by one-way ANOVA, ** P<0.01, **** P<0.0001 (bottom left). *C. rodentium* titers in feces measured as colony-forming units (CFU) of infected control and *CD11c.Bcl6*^{KO} mice at indicated days post infection; statistical analysis using Mann-Whitney test, not significant (right). All data points represent values from individual mice, lines represent the median and data is pooled from 2-3 experiments with 3-5 mice per mock/*C. rodentium* infected group.

D. H&E-stained sections of the distal colon of mock and *C. rodentium* infected control and *CD11c.Bcl6*^{KO} mice 21 days post inoculation. Scale bar, 100 µm. Symbols: # epithelial lining; ¤ leukocyte infiltration; % goblet cell destruction; & villus length. Representative of 4-5 mice per group from one experiment.

E. Numbers of total CD4^{+} T cells, IL-17A^{+}IL-22^{-}, IL-17A^{+}IL-22^{+}, IL-17A^{+}IFNγ^{-}, IL-17A^{+}IFNγ^{+} and Foxp3^{+} CD4^{+} T cells in the cLP of mock and *C. rodentium* infected control and *CD11c.Bcl6*^{KO} mice at day 9 post inoculation. Statistical analysis performed by one-way ANOVA, * P<0.05, ** P<0.01, *** P<0.001 and **** P<0.0001.

F. Numbers of total CD4^{+} T cells, IL-17A^{+}IL-22^{-}, IL-17A^{+}IL-22^{+}, IL-17A^{+}IFNγ^{-}, IL-17A^{+}IFNγ^{+} and Foxp3^{+} T cells in the cLP of mock and *C. rodentium* infected control and *CD11c.Bcl6*^{KO} mice at day 21 post inoculation. * P<0.05, ** P<0.01 and **** P<0.0001, by one-way ANOVA.

Figure 1

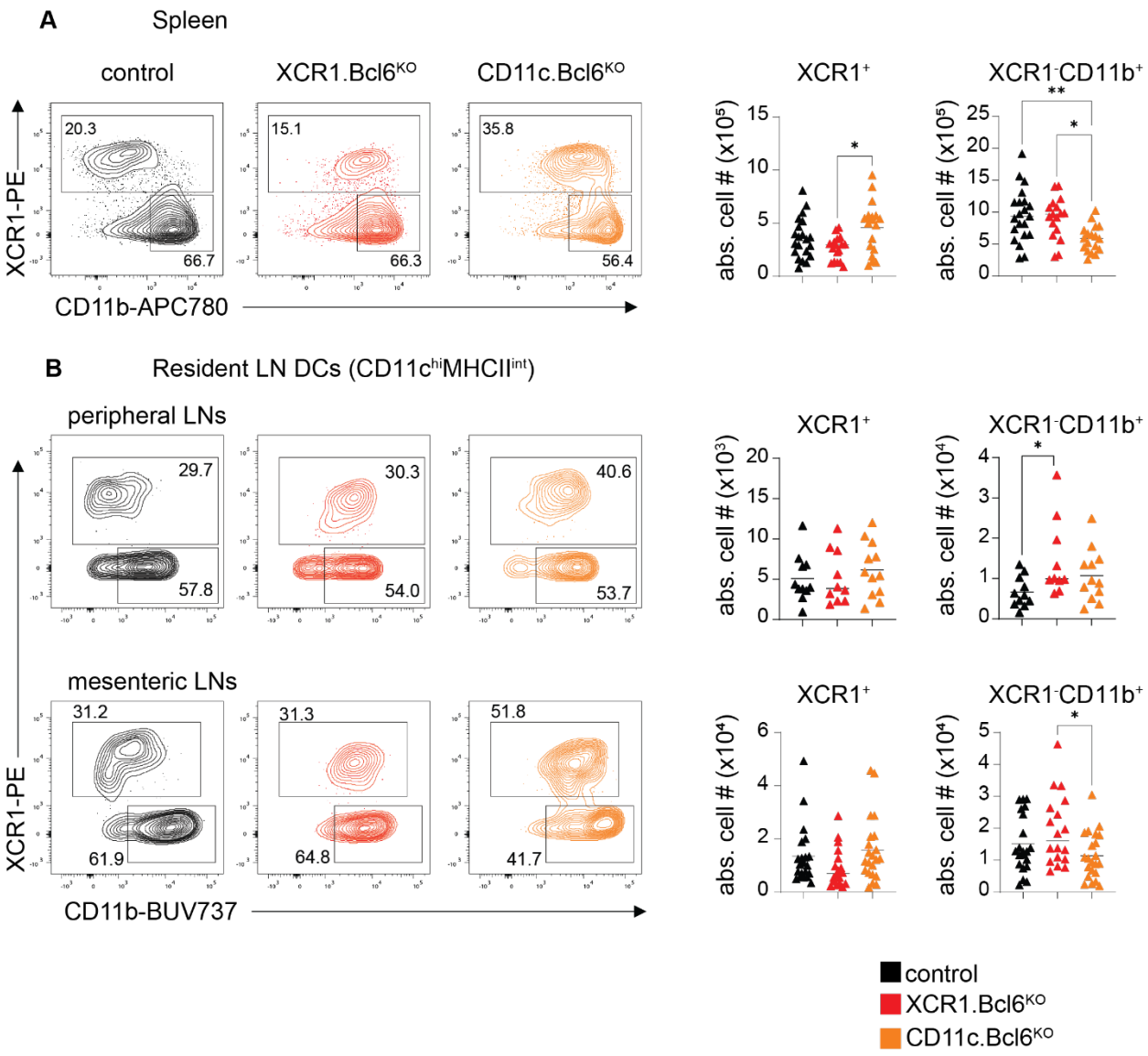
A
Spleen
control
XCR1.Bcl6KO
CD11c.Bcl6KO
XCR1-PE
CD11b-APC780
20.3
66.7
15.1
66.3
35.8
56.4
XCR1+
XCR1-CD11b+
abs. cell # (x10^5)
B
Resident LN DCs (CD11chiMHCIIint)
peripheral LNs
29.7
57.8
30.3
54.0
40.6
53.7
abs. cell # (x10^3)
abs. cell # (x10^4)
mesenteric LNs
31.2
61.9
31.3
64.8
51.8
41.7
CD11b-BUV737
control
XCR1.Bcl6KO
CD11c.Bcl6KO

Figure 2

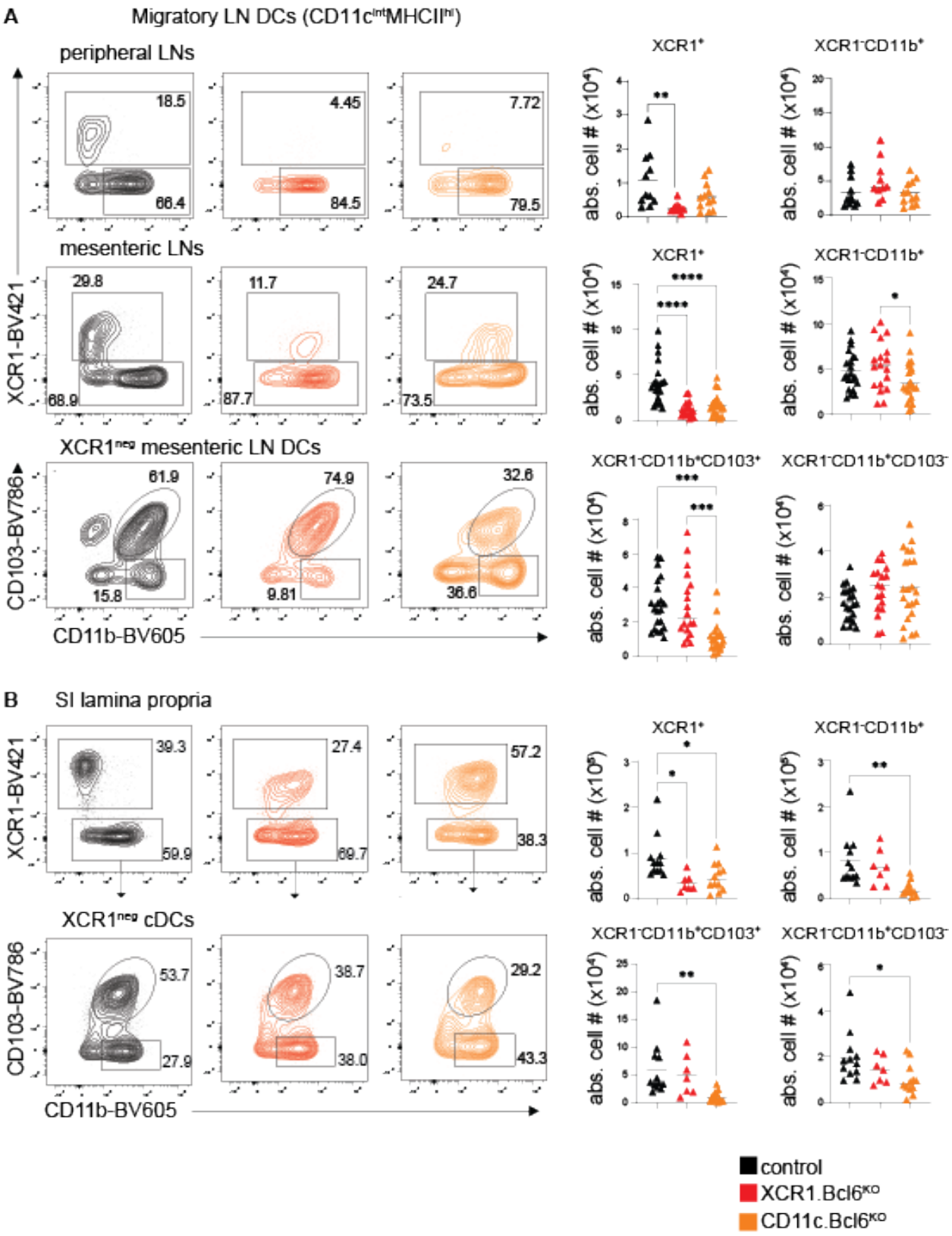
A
Migratory LN DCs (CD11c^int MHCII^hi)
peripheral LNs
mesenteric LNs
XCR1-BV421
XCR1^neg mesenteric LN DCs
CD103-BV786
CD11b-BV605
XCR1+
XCR1-CD11b+
XCR1-CD11b+CD103+
XCR1-CD11b+CD103-
abs. cell # (x10^4)
B
SI lamina propria
XCR1^neg cDCs
abs. cell # (x10^5)
control
XCR1.Bcl6^KO
CD11c.Bcl6^KO

Figure 3

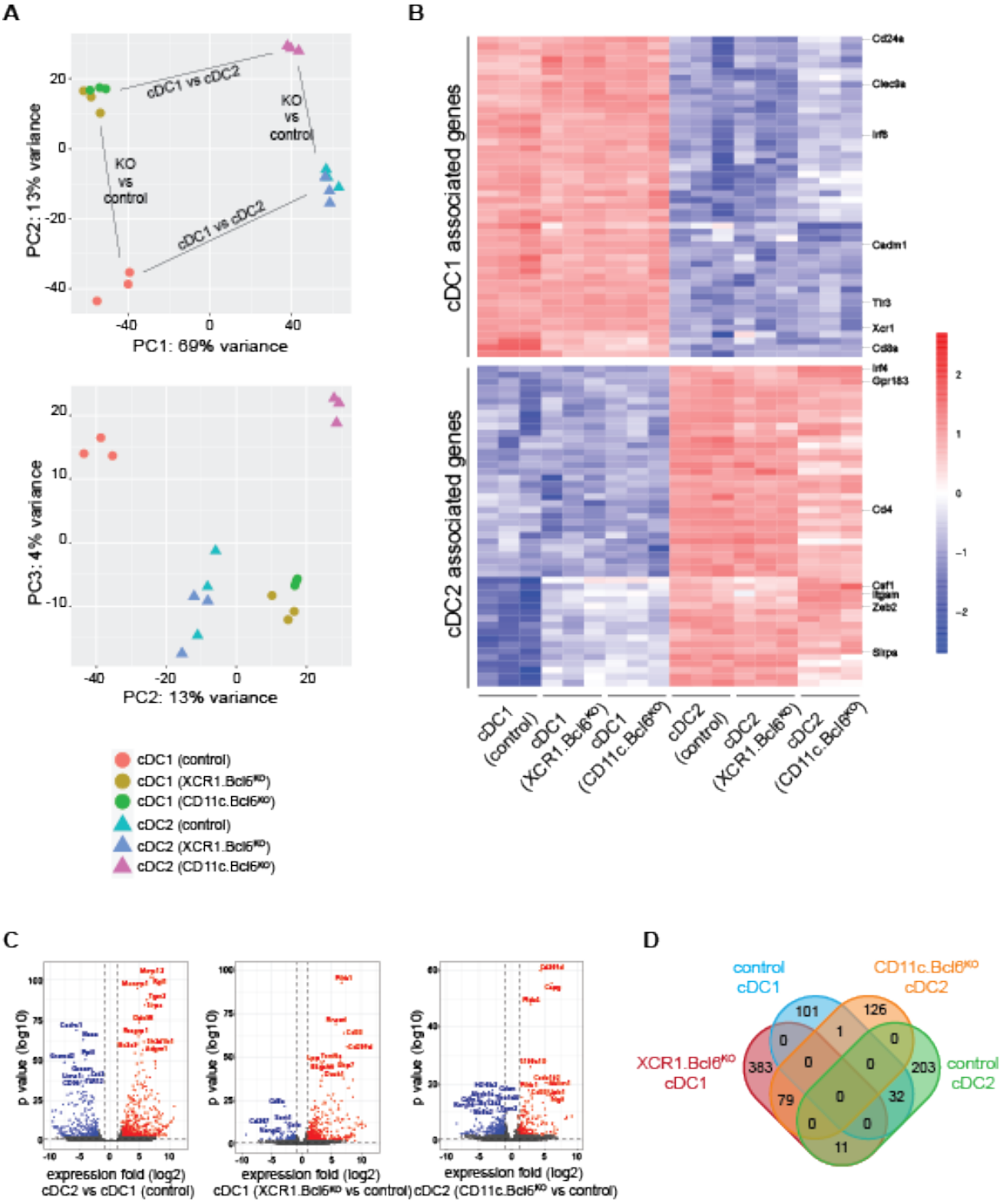
A
cDC1 vs cDC2
KO vs control
KO vs control
cDC1 vs cDC2
PC2: 13% variance
PC1: 69% variance
PC3: 4% variance
PC2: 13% variance
cDC1 (control)
cDC1 (XCR1.Bcl6KO)
cDC1 (CD11c.Bcl6KO)
cDC2 (control)
cDC2 (XCR1.Bcl6KO)
cDC2 (CD11c.Bcl6KO)
B
cDC1 associated genes
cDC2 associated genes
Cd24a
Clec9a
Irf8
Cadm1
Tlr3
Xcr1
Cd8a
Irf4
Gpr183
Cd4
Caf1
Itgam
Zeb2
Slfpa
cDC1 (control)
cDC1 (XCR1.Bcl6KO)
cDC1 (CD11c.Bcl6KO)
cDC2 (control)
cDC2 (XCR1.Bcl6KO)
cDC2 (CD11c.Bcl6KO)
C
p value (log10)
expression fold (log2)
cDC2 vs cDC1 (control)
cDC1 (XCR1.Bcl6KO vs control)
cDC2 (CD11c.Bcl6KO vs control)
D
control cDC1
CD11c.Bcl6KO cDC2
XCR1.Bcl6KO cDC1
control cDC2
101
126
1
0
0
383
0
0
203
79
0
32
0
0
11

Figure 4

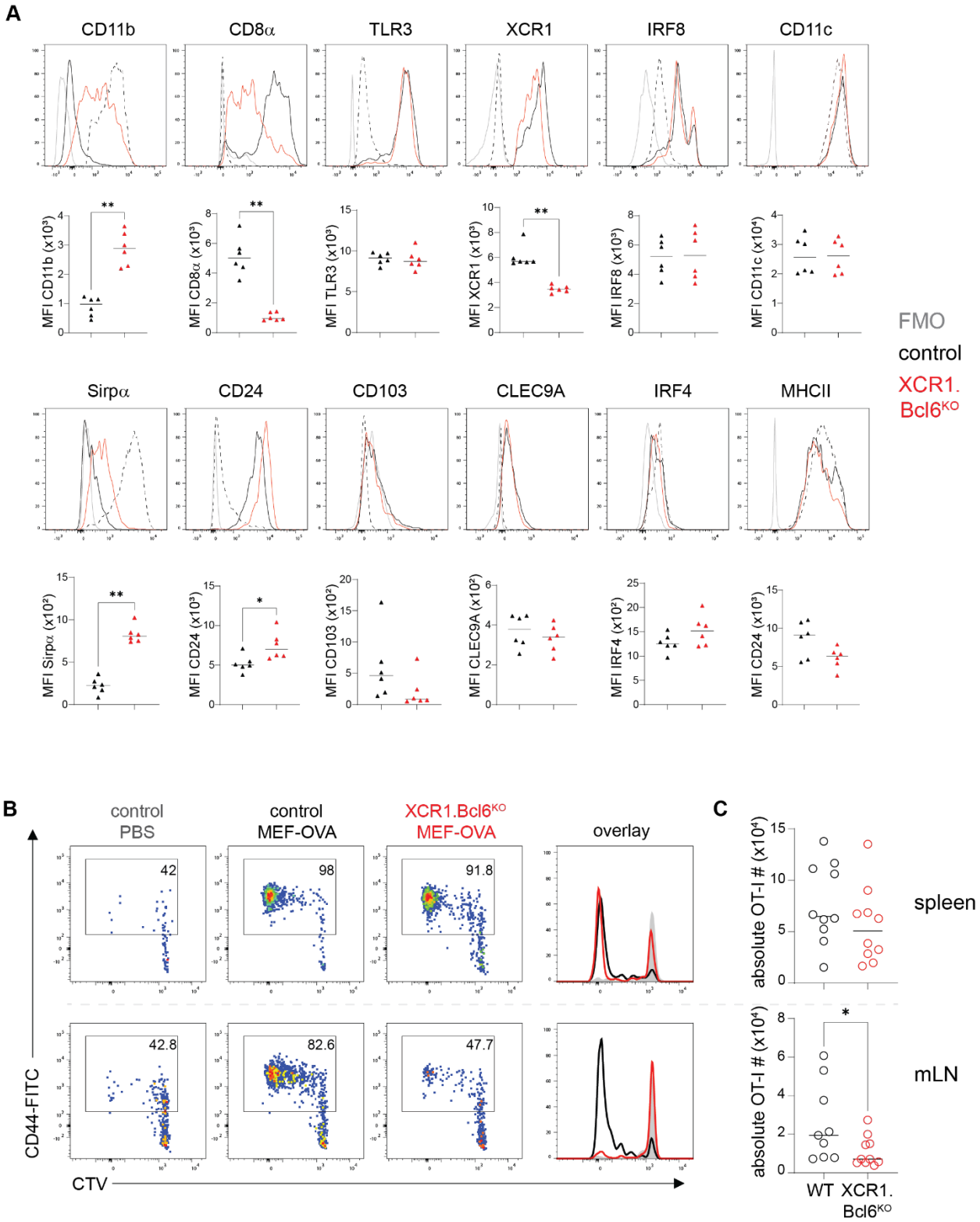
A
CD11b
CD8α
TLR3
XCR1
IRF8
CD11c
MFI CD11b (x10³)
MFI CD8α (x10³)
MFI TLR3 (x10³)
MFI XCR1 (x10³)
MFI IRF8 (x10³)
MFI CD11c (x10⁴)
FMO
control
XCR1.
Bcl6KO
Sirpα
CD24
CD103
CLEC9A
IRF4
MHCII
MFI Sirpα (x10²)
MFI CD24 (x10³)
MFI CD103 (x10²)
MFI CLEC9A (x10²)
MFI IRF4 (x10²)
MFI CD24 (x10³)
B
control
PBS
control
MEF-OVA
XCR1.Bcl6KO
MEF-OVA
overlay
42
98
91.8
42.8
82.6
47.7
CD44-FITC
CTV
C
absolute OT-I # (x10⁴)
spleen
mLN
WT
XCR1.
Bcl6KO

Figure 5

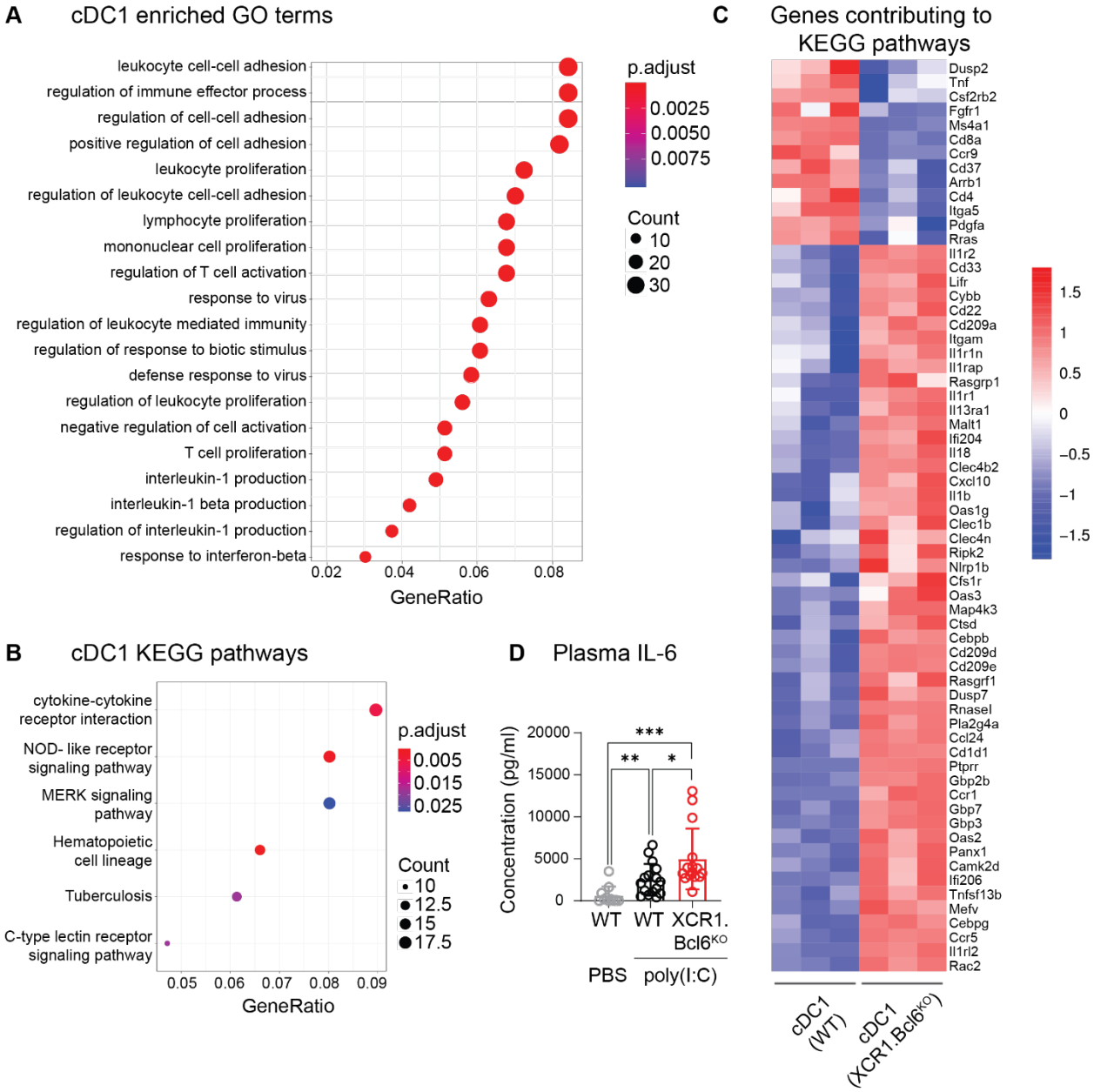
A
cDC1 enriched GO terms
leukocyte cell-cell adhesion
regulation of immune effector process
regulation of cell-cell adhesion
positive regulation of cell adhesion
leukocyte proliferation
regulation of leukocyte cell-cell adhesion
lymphocyte proliferation
mononuclear cell proliferation
regulation of T cell activation
response to virus
regulation of leukocyte mediated immunity
regulation of response to biotic stimulus
defense response to virus
regulation of leukocyte proliferation
negative regulation of cell activation
T cell proliferation
interleukin-1 production
interleukin-1 beta production
regulation of interleukin-1 production
response to interferon-beta
0.02
0.04
0.06
0.08
GeneRatio
p.adjust
0.0025
0.0050
0.0075
Count
10
20
30
B
cDC1 KEGG pathways
cytokine-cytokine receptor interaction
NOD- like receptor signaling pathway
MERK signaling pathway
Hematopoietic cell lineage
Tuberculosis
C-type lectin receptor signaling pathway
0.05
0.06
0.07
0.08
0.09
GeneRatio
p.adjust
0.005
0.015
0.025
Count
10
12.5
15
17.5
D
Plasma IL-6
Concentration (pg/ml)
20000
15000
10000
5000
0
***
**
*
WT
WT
XCR1.Bcl6KO
PBS
poly(I:C)
C
Genes contributing to KEGG pathways
Dusp2
Tnf
Csf2rb2
Fgfr1
Ms4a1
Cd8a
Ccr9
Cd37
Arrb1
Cd4
Itga5
Pdgfa
Rras
Il1r2
Cd33
Lifr
Cybb
Cd22
Cd209a
Itgam
Il1r1n
Il1rap
Rasgrp1
Il1r1
Il13ra1
Malt1
Ifi204
Il18
Clec4b2
Cxcl10
Il1b
Oas1g
Clec1b
Clec4n
Ripk2
Nlrp1b
Cfs1r
Oas3
Map4k3
Ctsd
Cebpb
Cd209d
Cd209e
Rasgrf1
Dusp7
RnaseI
Pla2g4a
Ccl24
Cd1d1
Ptprr
Gbp2b
Ccr1
Gbp7
Gbp3
Oas2
Panx1
Camk2d
Ifi206
Tnfsf13b
Mefv
Cebpg
Ccr5
Il1rl2
Rac2
1.5
1
0.5
0
−0.5
−1
−1.5
cDC1 (WT)
cDC1 (XCR1.Bcl6KO)

Figure 6

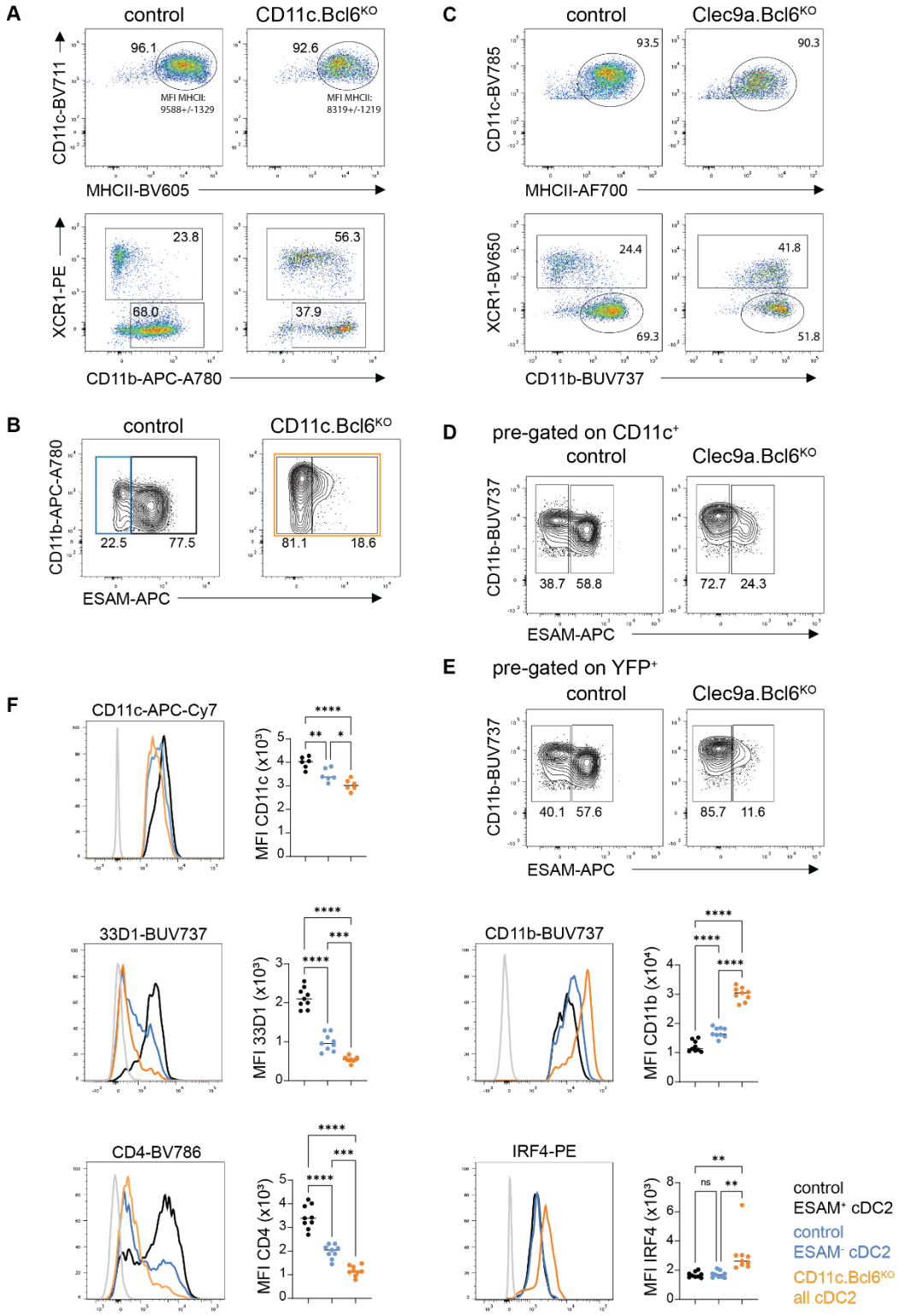
A
control
CD11c.Bcl6KO
96.1
92.6
MFI MHCII: 9588+/-1329
MFI MHCII: 8319+/-1219
CD11c-BV711
MHCII-BV605
23.8
68.0
56.3
37.9
XCR1-PE
CD11b-APC-A780
B
control
CD11c.Bcl6KO
CD11b-APC-A780
22.5
77.5
81.1
18.6
ESAM-APC
C
control
Clec9a.Bcl6KO
93.5
90.3
CD11c-BV785
MHCII-AF700
24.4
69.3
41.8
51.8
XCR1-BV650
CD11b-BUV737
D
pre-gated on CD11c+
control
Clec9a.Bcl6KO
CD11b-BUV737
38.7
58.8
72.7
24.3
ESAM-APC
E
pre-gated on YFP+
control
Clec9a.Bcl6KO
CD11b-BUV737
40.1
57.6
85.7
11.6
ESAM-APC
F
CD11c-APC-Cy7
MFI CD11c (x10³)
33D1-BUV737
MFI 33D1 (x10³)
CD11b-BUV737
MFI CD11b (x10⁴)
CD4-BV786
MFI CD4 (x10³)
IRF4-PE
MFI IRF4 (x10³)
ns
control ESAM+ cDC2
control ESAM- cDC2
CD11c.Bcl6KO all cDC2

Figure 7

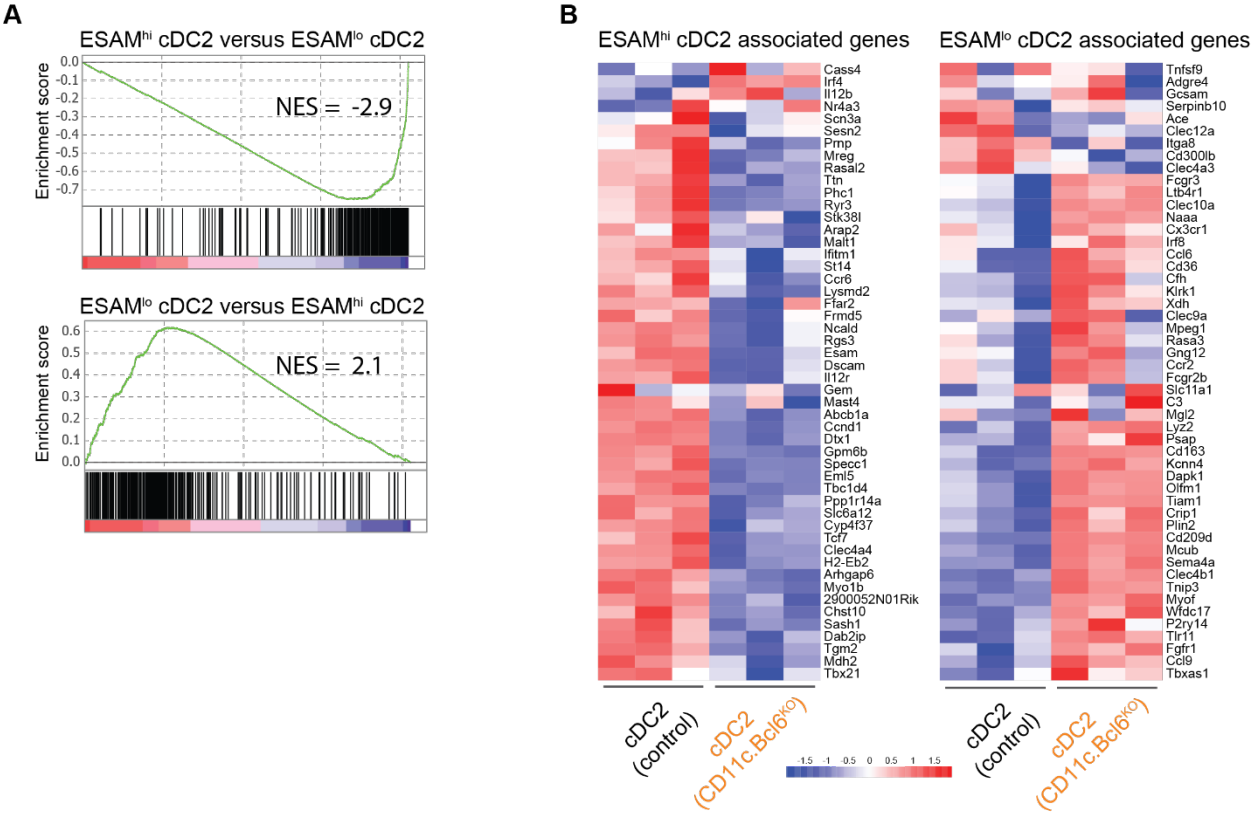
A
ESAMhi cDC2 versus ESAMlo cDC2
Enrichment score
NES = -2.9
ESAMlo cDC2 versus ESAMhi cDC2
Enrichment score
NES = 2.1
B
ESAMhi cDC2 associated genes
ESAMlo cDC2 associated genes
Cass4
Irf4
Il12b
Nr4a3
Scn3a
Sesn2
Prnp
Mreg
Rasal2
Ttn
Phc1
Ryr3
Stk38l
Arap2
Malt1
Ifitm1
St14
Ccr6
Lysmd2
Ffar2
Frmd5
Ncald
Rgs3
Esam
Dscam
Il12r
Gem
Mast4
Abcb1a
Ccnd1
Dtx1
Gpm6b
Specc1
Eml5
Tbc1d4
Ppp1r14a
Slc6a12
Cyp4f37
Tcf7
Clec4a4
H2-Eb2
Arhgap6
Myo1b
2900052N01Rik
Chst10
Sash1
Dab2ip
Tgm2
Mdh2
Tbx21
Tnfsf9
Adgre4
Gcsam
Serpinb10
Ace
Clec12a
Itga8
Cd300lb
Clec4a3
Fcgr3
Ltb4r1
Clec10a
Naaa
Cx3cr1
Irf8
Ccl6
Cd36
Cfh
Klrk1
Xdh
Clec9a
Mpeg1
Rasa3
Gng12
Ccr2
Fcgr2b
Slc11a1
C3
Mgl2
Lyz2
Psap
Cd163
Kcnn4
Dapk1
Olfm1
Tiam1
Crip1
Plin2
Cd209d
Mcub
Sema4a
Clec4b1
Tnip3
Myof
Wfdc17
P2ry14
Tlr11
Fgfr1
Ccl9
Tbxas1
cDC2 (control)
cDC2 (CD11c.Bcl6KO)
cDC2 (control)
cDC2 (CD11c.Bcl6KO)

Figure 8

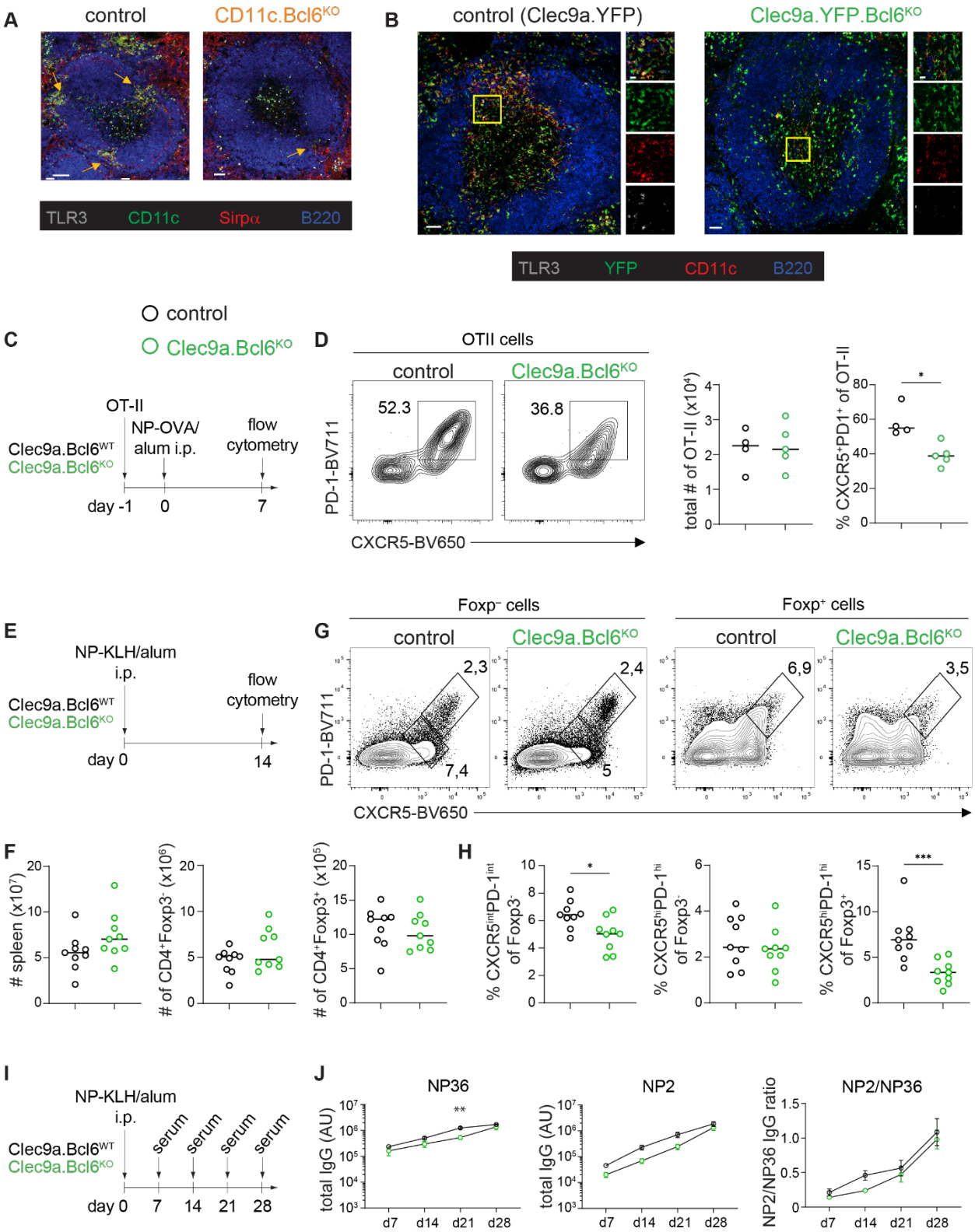
A
control
CD11c.Bcl6KO
TLR3
CD11c
Sirpα
B220
B
control (Clec9a.YFP)
Clec9a.YFP.Bcl6KO
TLR3
YFP
CD11c
B220
C
control
Clec9a.Bcl6KO
OT-II
NP-OVA/
alum i.p.
flow
cytometry
Clec9a.Bcl6WT
Clec9a.Bcl6KO
day -1
0
7
D
OTII cells
control
Clec9a.Bcl6KO
52.3
36.8
PD-1-BV711
CXCR5-BV650
total # of OT-II (x10⁴)
% CXCR5+PD1+ of OT-II
E
NP-KLH/alum
i.p.
flow
cytometry
Clec9a.Bcl6WT
Clec9a.Bcl6KO
day 0
14
G
Foxp− cells
Foxp+ cells
control
Clec9a.Bcl6KO
2,3
7,4
2,4
5
6,9
3,5
PD-1-BV711
CXCR5-BV650
F
spleen (x10⁷)
of CD4+Foxp3- (x10⁶)
# of CD4+Foxp3+ (x10⁵)
H
% CXCR5intPD-1int of Foxp3-
% CXCR5hiPD-1hi of Foxp3-
% CXCR5hiPD-1hi of Foxp3+
I
NP-KLH/alum
i.p.
serum
serum
serum
serum
Clec9a.Bcl6WT
Clec9a.Bcl6KO
day 0
7
14
21
28
J
NP36
NP2
NP2/NP36
total IgG (AU)
NP2/NP36 IgG ratio
d7
d14
d21
d28

Figure 9

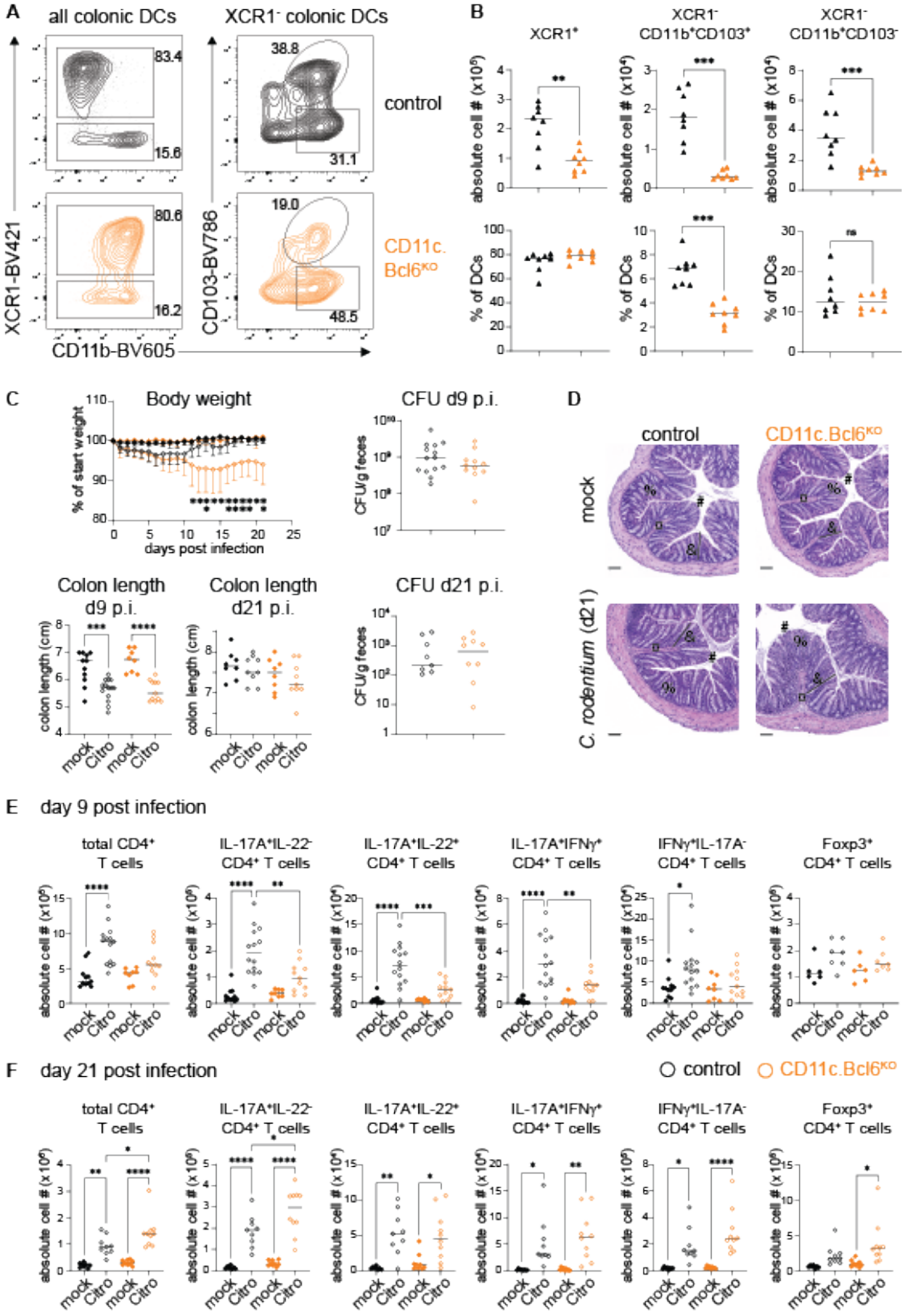
A
all colonic DCs
XCR1⁻ colonic DCs
control
CD11c.Bcl6KO
XCR1-BV421
CD11b-BV605
CD103-BV786
B
XCR1⁺
XCR1⁻ CD11b⁺CD103⁺
XCR1⁻ CD11b⁺CD103⁻
absolute cell # (x10⁶)
% of DCs
C
Body weight
% of start weight
days post infection
CFU d9 p.i.
CFU/g feces
Colon length d9 p.i.
Colon length d21 p.i.
colon length (cm)
CFU d21 p.i.
mock
Citro
D
control
CD11c.Bcl6KO
mock
C. rodentium (d21)
E day 9 post infection
total CD4⁺ T cells
IL-17A⁺IL-22⁻ CD4⁺ T cells
IL-17A⁺IL-22⁺ CD4⁺ T cells
IL-17A⁺IFNγ⁺ CD4⁺ T cells
IFNγ⁺IL-17A⁻ CD4⁺ T cells
Foxp3⁺ CD4⁺ T cells
absolute cell # (x10⁶)
F day 21 post infection
control
CD11c.Bcl6KO

Supplementary Figure 1

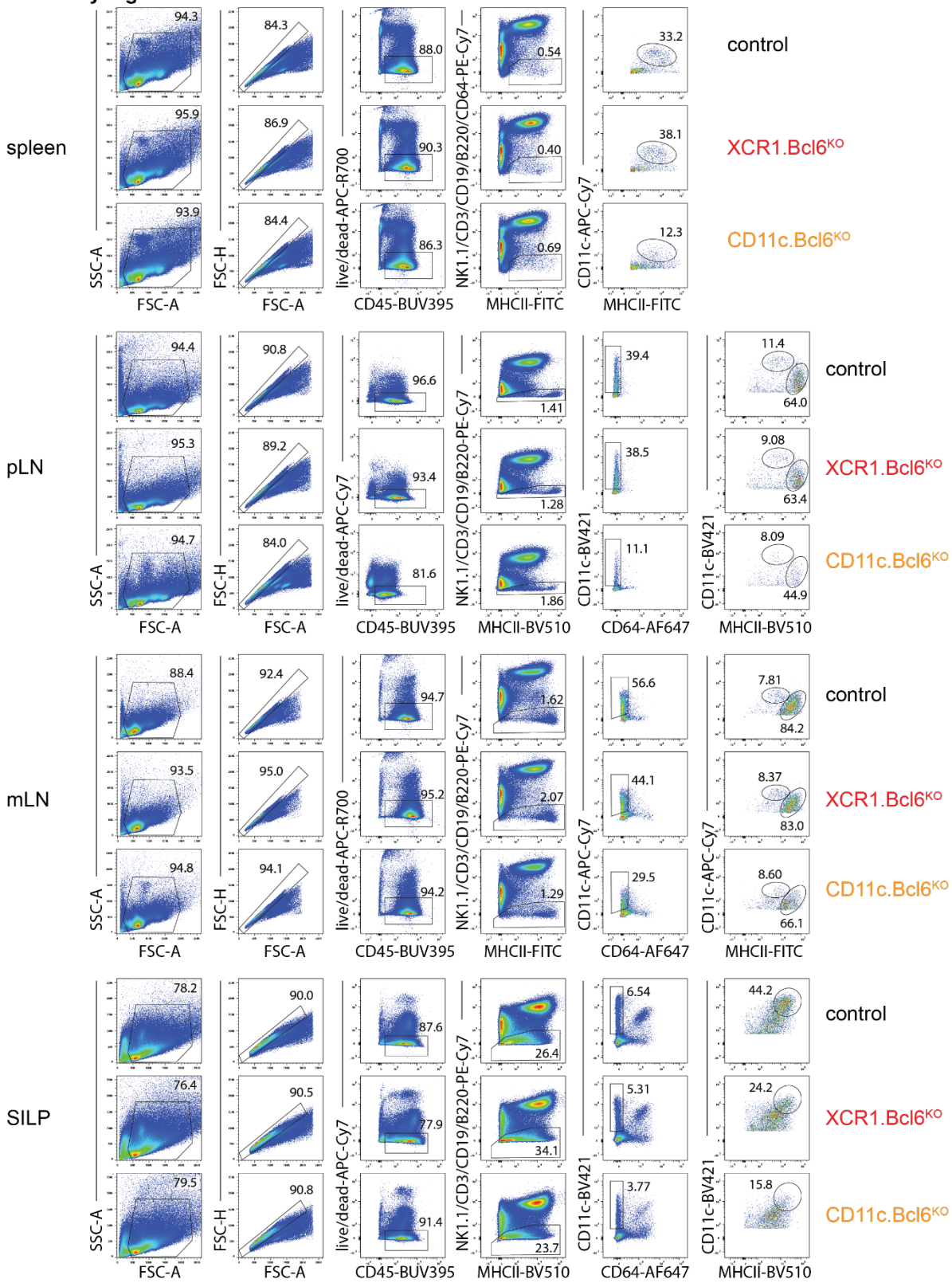

Supplementary Figure 1: Full gating strategy for spleen, pLN, mLN and SILP cDC from control, *XCR1.Bcl6^{KO}*,

and *CD11c.Bcl6*^{KO} mice.

Supplementary Figure 2

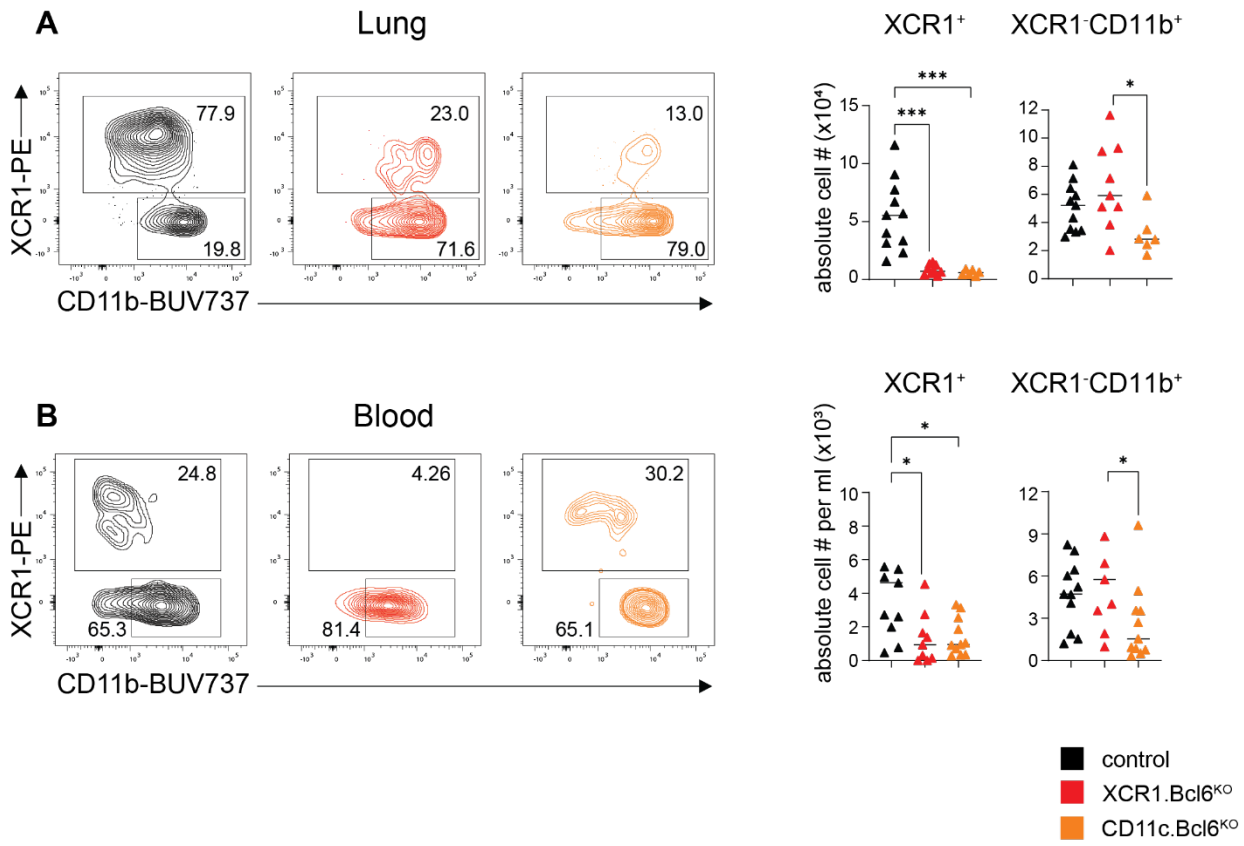

Supplementary Figure 2

A. Left: Flow cytometry plots show XCR1^{+} and XCR1^{-}CD11b^{+} DC subsets in the lungs of control, *XCR1.Bcl6*^{KO} and *CD11c.Bcl6*^{KO} mice. The plots show representative staining profiles of live, CD45^{+}, lineage^{-} (CD3, CD19, CD64, B220, NK1.1), MHCII^{+}, CD11c^{hi} gated single cells. Right: Absolute numbers of cDC subsets in the lungs of control, *XCR1.Bcl6*^{KO}, and *CD11c.Bcl6*^{KO} mice. Statistical analysis by one-way ANOVA.** P<0.01, **** P<0.0001. Data points represent values from individual mice pooled from 2-3 experiments and lines represent the medians.

B. Left: Representative flow cytometry plots of blood XCR1^{+} and XCR1^{-}CD11b^{+} DC subsets from control, XCR1.Bcl6^{KO} and CD11c.Bcl6^{KO}. Shown are representative staining profiles of live, CD45^{+},

lineage^{-} (CD3, CD19, CD64, B220, NK1.1), MHCII^{+}, CD11c^{hi} gated single cells. Right: Absolute numbers of cDC1 and cDC2 in blood of control, XCR1.Bcl6^{KO}, and CD11c.Bcl6^{KO} mice. Statistical analysis by one-way ANOVA, significance at * $P<0.05$. Data points are normalized to volume of blood drawn and represent values from individual mice pooled from 4 experiments; lines represent the median cell numbers from each genotype.

Supplementary Figure 3

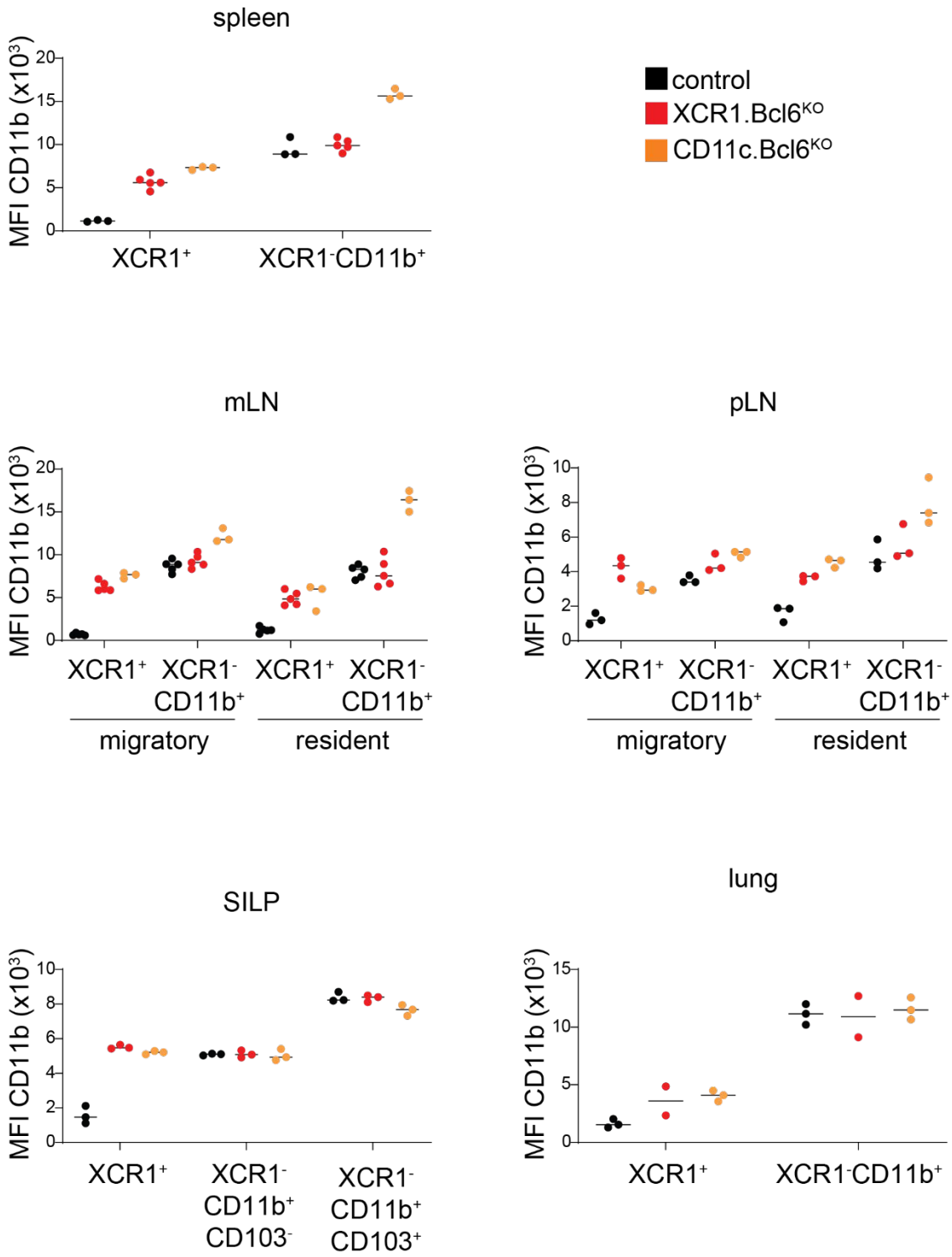

Supplementary Figure 3

Raw values of CD11b MFI in XCR1$^+$ and XCR1$^-$CD11b$^+$ (spleen, mLN, pLN and lung) or XCR1$^+$ and XCR1$^-$ CD11b$^+$CD103$^-$ and CD11b$^+$CD103$^+$ (SILP) cDC from control, *XCR1.Bcl6^{KO}*, and *CD11c.Bcl6^{KO}* mice. Note that different organs were stained using different panels and CD11b MFI values are therefore not comparable across organs. Data depicts one representative experiment of at least 3 per organ with 2-3 mice each.

Supplementary Figure 4

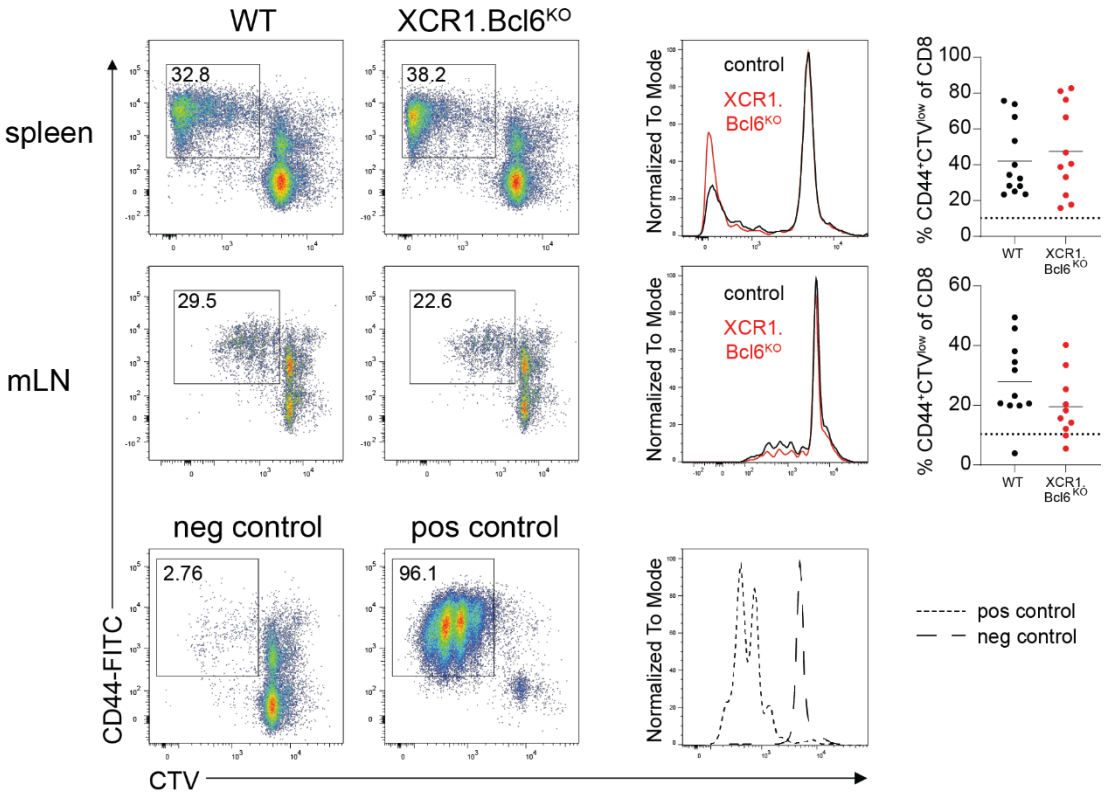

Supplementary Figure 4

Representative flow cytometry plots showing CTV dilution and CD44 expression on OT-I cells (gated on live, CD11c$^-$, CD8α$^+$ single cells) following 65h incubation with OVA pulsed and LPS stimulated cDC1 isolated from spleen (top) and mLN (bottom) of control and *XCR1.Bcl6^{KO}* mice. Data are representative of four independent experiments with 2-3 mice each.

Histograms show CTV dilution in OT-I cells after incubation with OVA pulsed cDC1 isolated from spleen and mLN of control and *XCR1.Bcl6^{KO}* mice. Bottom histogram shows CTV dilution in OT-I cells after incubation with anti-CD3 and anti-CD28 (positive control) and non-pulsed cDC1 (negative control).

Percentage of CD44^{+} CTV^{low} OT-I cells after incubation with cDC1s isolated from spleen and mLN of control and *XCR1.Bcl6^{KO}* mice. Data is pooled from four independent experiments. Each dot represents one mouse, solid lines represent the medians and dotted lines represent the average percentage of CD44^{+} CTV^{low} OT-I cells from negative controls across all independent experiments.

Supplementary Figure 5

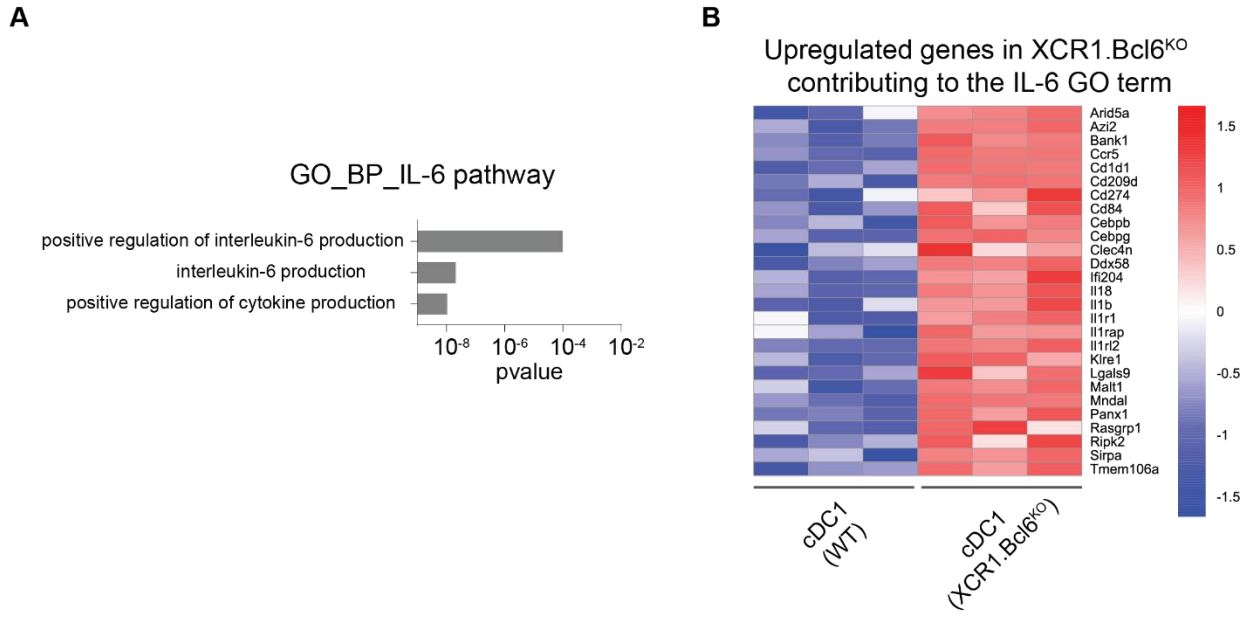

Supplementary Figure 5

A. IL-6 pathway gene ontology (GO) term enrichment analysis of differentially expressed genes (DEGs) in *XCR1.Bcl6^{KO}* and control cDC1. The p value calculated from GO term enrichment analysis is represented on the x-axis and the y-axis shows the GO Biological Process (BP) terms. Only terms related to positive regulation of IL-6 production are depicted.

B. Heatmap of all upregulated genes in *XCR1.Bcl6*^{KO} cDC1 contributing to the enriched IL-6 pathways depicted in A. The color scale represents the row Z score.

Supplementary Figure 6

A Relative abundance of cDC subsets in the spleen in Clec9a.Bcl6^{KO} and CD11c.Bcl6^{KO} mice

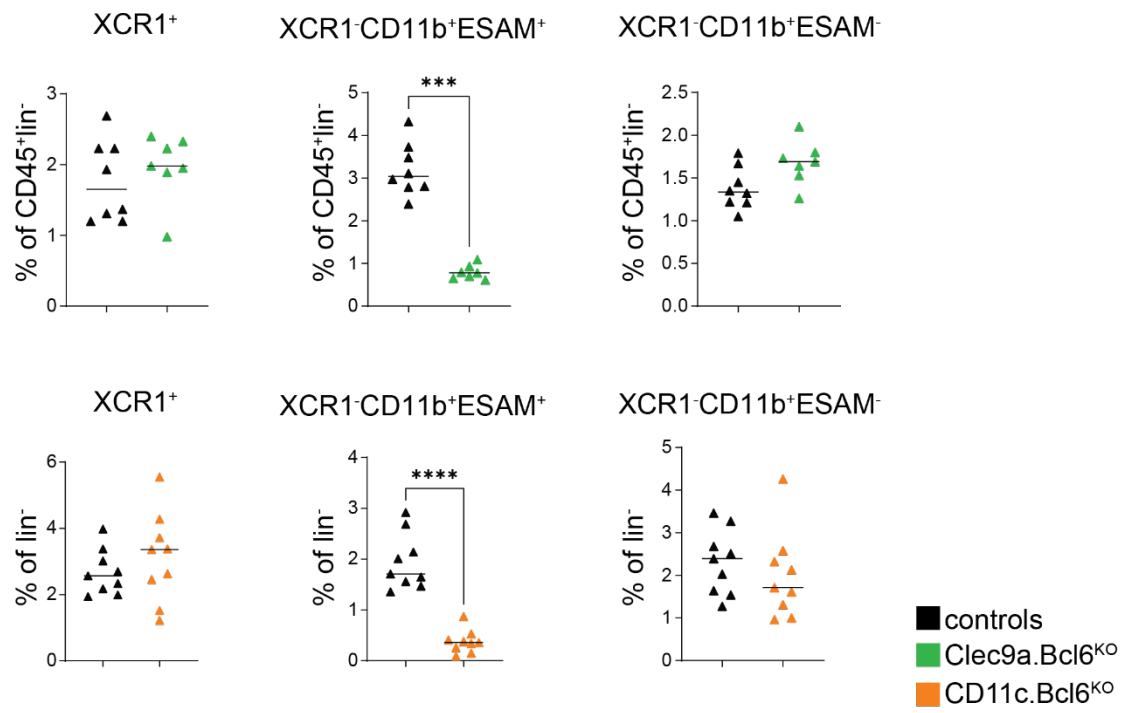

B Absolute count of cDC subsets in the spleen in Clec9a.Bcl6^{KO} and CD11c.Bcl6^{KO} mice

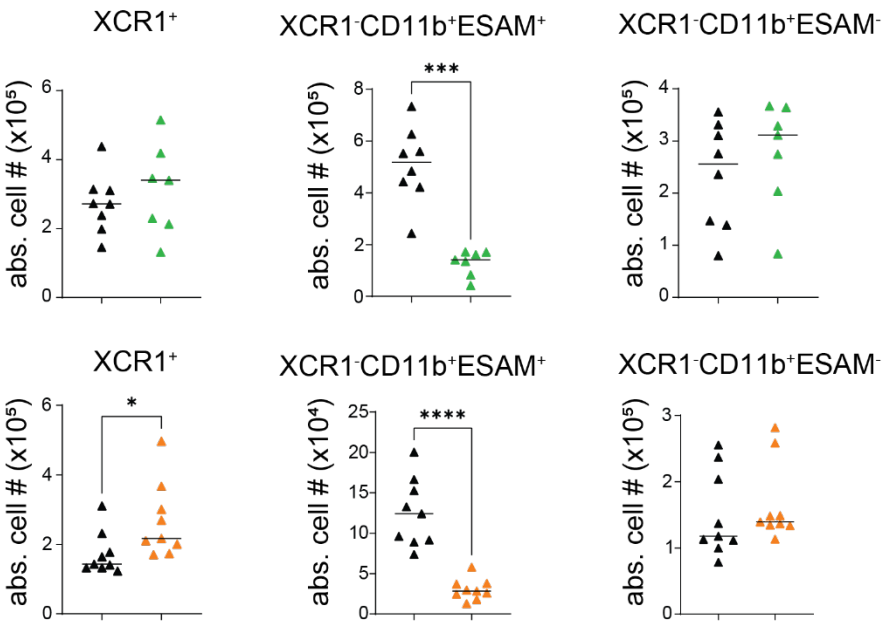

Supplementary Figure 6

A. Relative proportions of XCR1^{+}, XCR1^{-}CD11b^{+}ESAM^{hi} and XCR1^{-}CD11b^{+}ESAM^{lo} subsets in the spleen of Clec9a.*Bcl6*^{KO} (top) and CD11c.*Bcl6*^{KO} (bottom) mice. Cells were pre-gated on single live, CD45^{+}, lineage^{-} (CD3, CD19, TER119, B220, NK1.1), MHCII^{+}, CD11c^{hi}. Data points represent values from individual mice pooled from 2-3 experiments and lines represent the medians. Statistical analysis using Mann-Whitney test, *** P<0.001 and **** P<0.0001.

B. Numbers of XCR1^{+}, XCR1^{-}CD11b^{+}ESAM^{hi} and XCR1^{-}CD11b^{+}ESAM^{lo} subsets in the spleen of control, Clec9a.*Bcl6*^{KO} normalized to volume of suspension (top) and CD11c.*Bcl6*^{KO} shown as absolute numbers (bottom). Data points represent values from individual mice pooled from 2-3 experiments and lines represent the medians. * P<0.05, *** P<0.001 and **** P<0.0001, by Mann-Whitney test.

Supplementary Figure 7

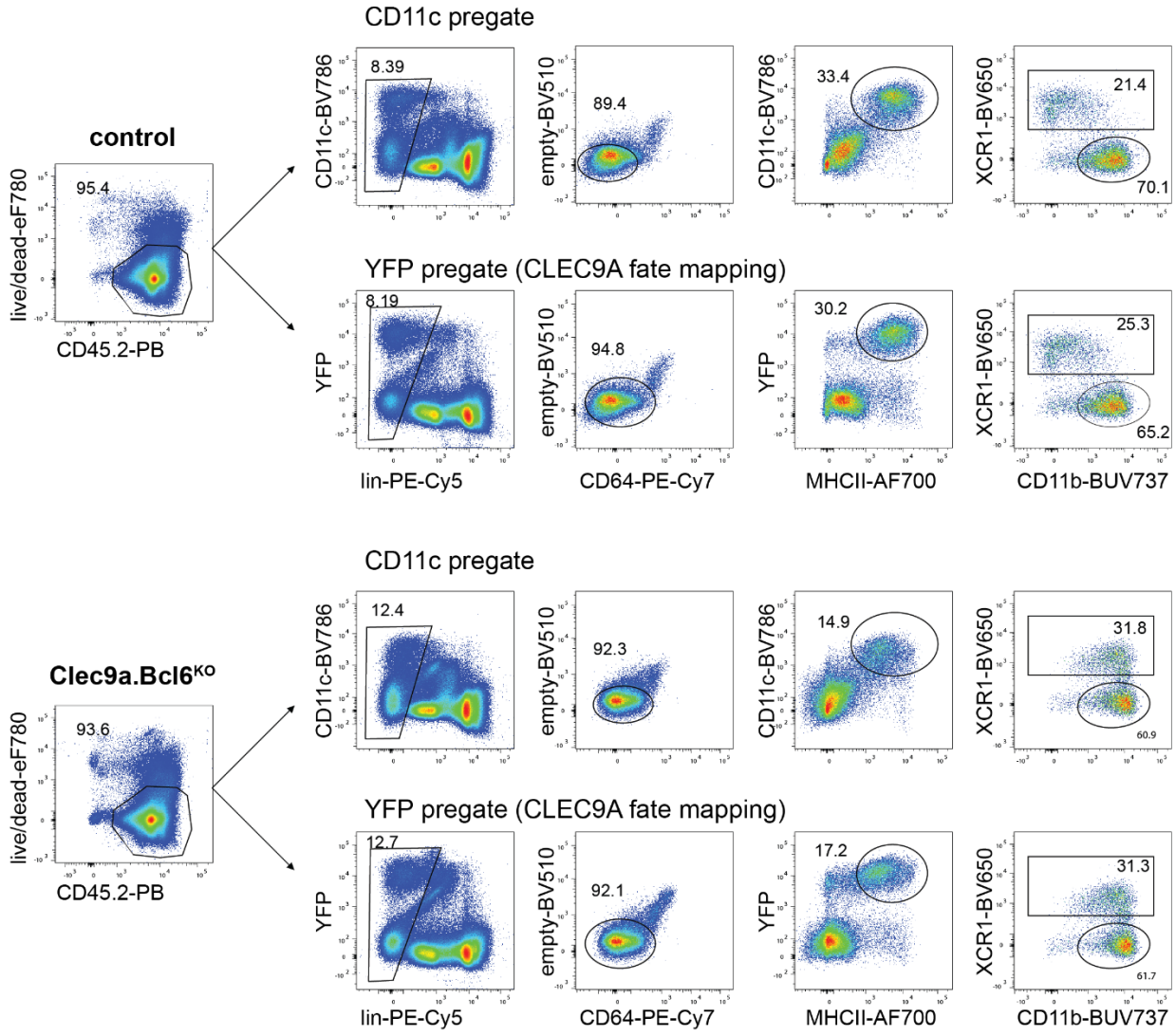

Supplementary Figure 7

FACS plots showing alternative gating strategies for cDCs in Clec9a.*Bcl6*^{KO} and control mice. CD11c pre-gate: classical CD11c-based gating; YFP pre-gate: Gating based on *Clec9a* fate mapping (Clec9a.*Bcl6*^{KO} mice contain the *R26-ROSA*^{YFP} locus). Data is representative for 3 experiments with 2-3 mice each.

Supplementary Figure 8

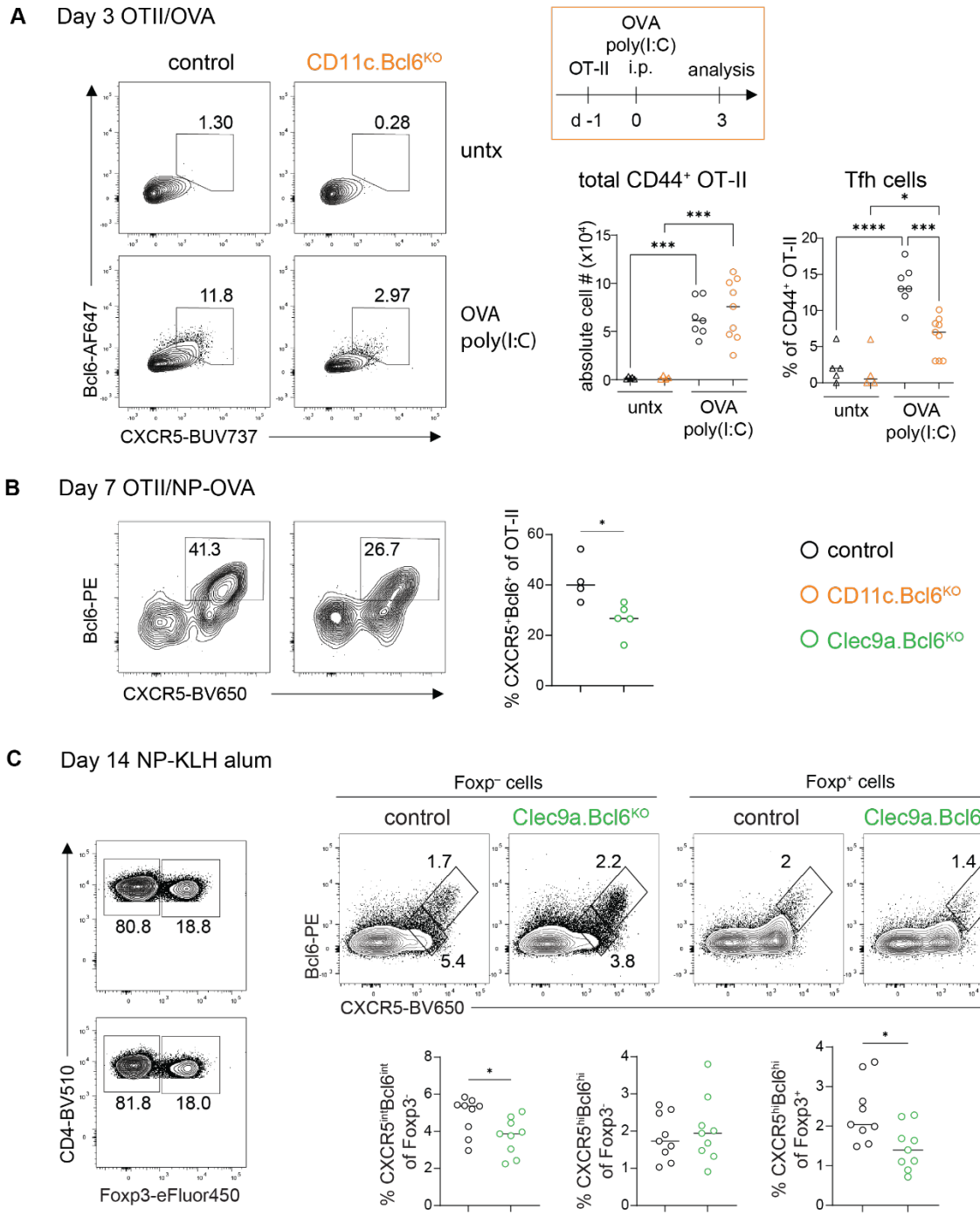

Supplementary Figure 8

A. Representative flow cytometric analysis of early Tfh cell induction amongst OT-II cells in the spleen of control and *CD11c.Bcl6*^{KO} mice 3 days after i.p. immunization with OVA and poly(I:C) or with PBS as a control. Tfh were gated as live CD4^{+}Vβ5.2^{+}CD45.1^{+}CD45.2^{+}CD44^{+}Bcl6^{+}CXCR5^{+} and the results are representative of three experiments with 3-5 mice each. Right: Numbers of total CD44^{+} OT-II T cells (left panel), left: proportions (right panel) of OVA-specific Tfh cells in the spleens of control and *CD11c.Bcl6*^{KO} mice 3 days after i.p. immunization with OVA and poly(I:C) or with PBS as a control. Statistical analysis was performed by one-way ANOVA. * P<0.05, ** P<0.01, *** P<0.001 and **** P<0.0001. Data points represent values from individual mice pooled from three experiments with 3-5 mice each in OVA/poly(I:C) immunized groups. Each experiment contained at least one untreated control per genotype; lines represent the medians.
B. Bcl6-staining and Bcl6-based quantification of Tfh cells of data presented in Figure 8C, D.
C. Foxp3-staining of CD4^{+} T cells and Bcl6-staining and Bcl6-based quantification of Tfh cells, GC Tfh cells, and Tfr cells complementary to data presented in Figure 8E to H.
D. NP-specific IgG1 antibody titers accompanying total IgG data presented in Figure 8I, J.

Supplementary Figure 9

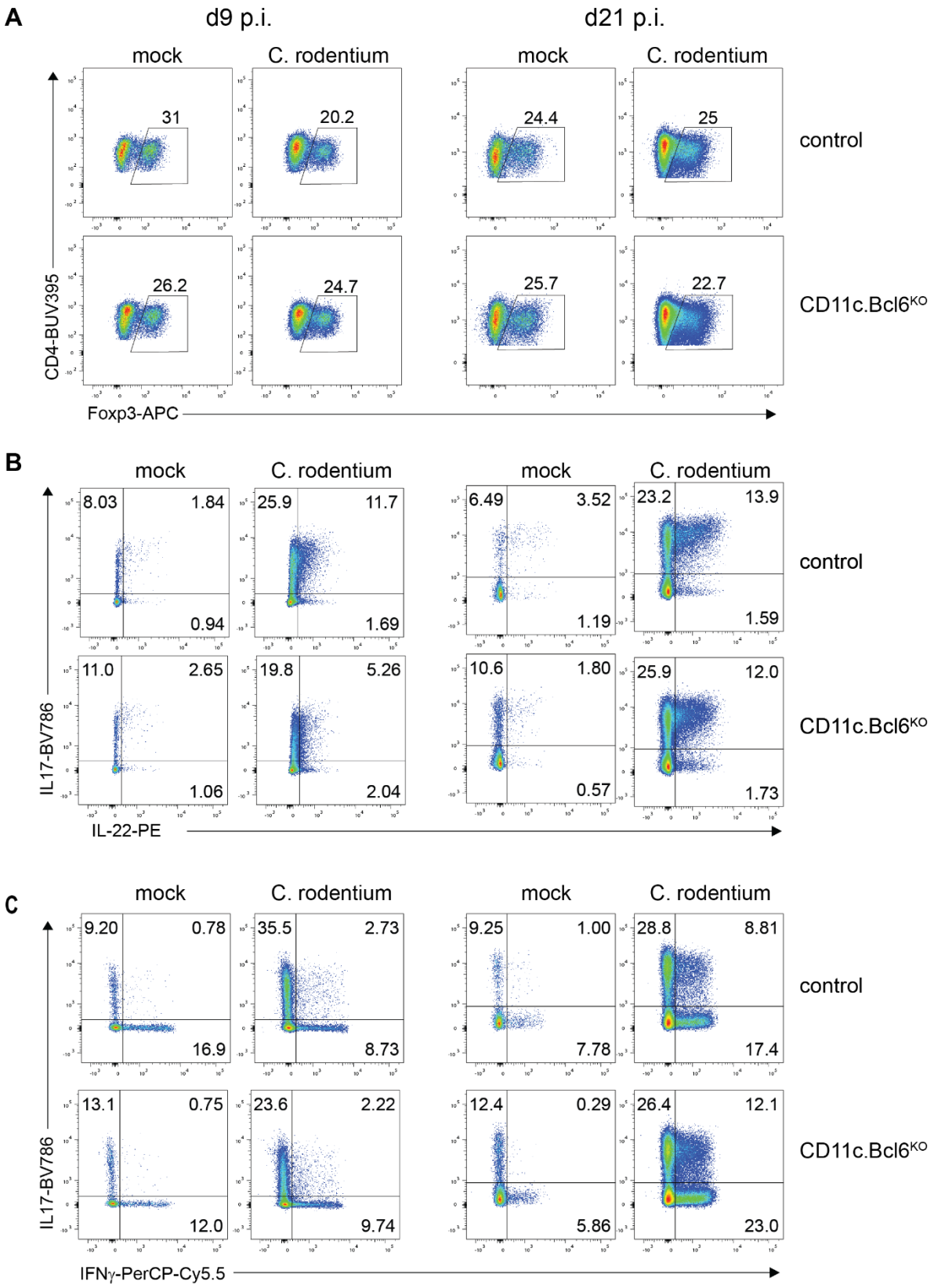

Supplementary Figure 9

A. Representative flow cytometry plots showing Foxp3$^+$ CD4$^+$ T cells (gated on live, CD45$^+$, CD3$^+$TCRβ$^+$ singlets) in the cLP of mock and C. rodentium infected control and CD11c.Bcl6^{KO} mice at day 9 (left) or day 21 (right) post inoculation.

B. Representative flow cytometry analysis showing IL-17A$^+$IL-22$^+$ CD4$^+$ T cells (gated on live, CD45$^+$, CD3$^+$TCRβ$^+$ singlets) in the cLP of mock and C. rodentium infected control and CD11c.Bcl6^{KO} mice at day 9 (left) or day 21 (right) post inoculation.

C. Representative flow cytometry plots showing IL-17A$^+$IFNγ$^+$ CD4$^+$ T cells (gated on live, CD45+, CD3$^+$TCRβ$^+$ singlets) in the cLP of mock and C. rodentium infected control and CD11c.Bcl6^{KO} mice at day 9 (left) or day 21 (right) post inoculation.

Supplementary Figure 10

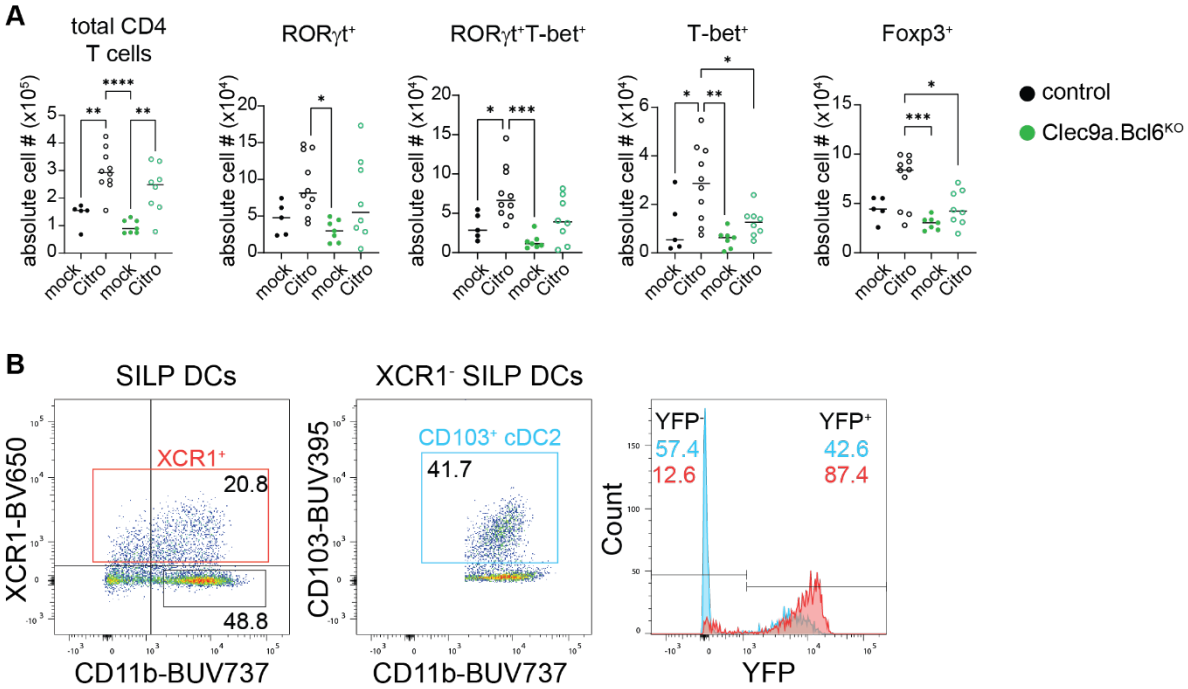

Supplementary Figure 10

A. Numbers of total CD4$^+$ T cells, RORgt$^+$, RORgt$^+$T-bet$^+$, T-bet$^+$, and Foxp3$^+$ CD4$^+$ T cells in the cLP of mock and *C. rodentium* infected control and *Clec9a.Bcl6^{KO}* mice at day 9 post inoculation.

Statistical analysis performed by one-way ANOVA, * $P<0.05$, ** $P<0.01$, *** $P<0.001$ and **** $P<0.0001$. Data representative of 3 independent experiments with 1-3 mice each.

B. Left: Flow cytometry plot showing $XCR1^+$ and $XCR1^-CD11b^+$ gating on SILP DCs, pre-gated on live, $lineage^-$ (CD3, CD19, CD64, B220, NK1.1), $CD11c^+$, $MHCII^+$ single cells; right: Sub-gate on $XCR1^-CD11b^+$ cells. Histogram shows YFP-expression in XCR1+ cDC1 (red) and $XCR1^-CD11b^+CD103^+$ cDC2 (blue). Data representative of 2 experiments with 3 mice each.